Machinability study of flame sprayed Hydroxyapatite Coating deposited on Ti-6AL-4V substrates

M. Tech Thesis

By

Lalit Tyagi

(2402103012)



DEPARTMENT OF MECHANICAL ENGINEERING

INDIAN INSTITUTE OF TECHNOLOGY INDORE

June 2026

Machinability study of flame sprayed Hydroxyapatite Coating deposited on Ti-6AL-4V substrates

A THESIS

Submitted in partial fulfillment of the
requirements for the award of the degree
of
Master of Technology

by
Lalit Tyagi



DEPARTMENT OF MECHANICAL ENGINEERING
INDIAN INSTITUTE OF TECHNOLOGY INDORE
June 2026

INDIAN INSTITUTE OF TECHNOLOGY INDORE

CANDIDATE'S DECLARATION

I hereby certify that the work which is being presented in the thesis entitled **Machinability study of flame sprayed Hydroxyapatite Coating deposited on Ti-6AL-4V substrates** in the partial fulfillment of the requirements for the award of the degree of **MASTER OF TECHNOLOGY** and submitted in the **DEPARTMENT OF MECHANICAL ENGINEERING, Indian Institute of Technology Indore**, is an authentic record of my own work carried out during the time period from July 2024 to June 2026 under the supervision of Dr. Kazi Sabiruddin, Professor, Department of Mechanical Engineering.

The matter presented in this thesis has not been submitted by me for the award of any other degree of this or any other institute.

Lalit Tyagi 26/05/26
Signature of the student with date
Lalit Tyagi

This is to certify that the above statement made by the candidate is correct to the best of my/our knowledge.

26/05/26
Signature of the Supervisor of
M. Tech. thesis (with date)
Prof. Kazi Sabiruddin

Lalit Tyagi has successfully given his M. Tech. Oral Examination held on 26th May 2026.

Signature of Supervisor of M. Tech thesis
Date: 26th May 2026

Convener, DPGC
Date: 26th May 2026

ACKNOWLEDGEMENTS

I would like to express my deepest gratitude and appreciation to my supervisor, Prof. Kazi Sabiruddin, of the Department of Mechanical Engineering, Indian Institute of Technology Indore, for his invaluable guidance, support, patience, and mentorship throughout my project work. I sincerely thank him for granting me the opportunity to work under his guidance.

I would also like to thank my seniors Mr. Setu Suman, Mr. Ashok Kumar and other lab members for their invaluable support and contributions throughout this research.

Lastly, I would like to acknowledge the IIT Indore, M & T Laboratory, Thermal Spraying Laboratory, Workshop and SIC, whose support made this research possible.

The people with the greatest indirect contribution to this work are my parents, who have been with me constantly and encouraged me throughout this work and in life as well. Without their support, this thesis would not have been possible.

With Regards

Lalit Tyagi

Dedicated to my loving and caring parents.

ABSTRACT

Hydroxyapatite (HA) is a preferred coating material for orthopedic and dental implants due to its biocompatibility, osteoconductivity, and bioactivity. Surface coating technology, particularly thermal spray techniques such as flame spraying, enables the deposition of bioactive ceramic coatings on metallic implant substrates. Ti-6Al-4V alloy serves as the structural substrate owing to its high specific strength, corrosion resistance, and proven biocompatibility, though its bio-inert nature necessitates surface modification. Post-deposition machining of these coatings is essential for achieving precise dimensional accuracy and geometric features required for patient-specific implant fitment. In this work, seashell-derived HA powder was synthesized by the hydrothermal method, and commercial HA powder was also procured. Both powders were deposited on Ti-6Al-4V substrates using flame spraying at three standoff distances (70, 90, and 110 mm). The coatings were characterized for thickness (236.79–369.28 μm) and surface roughness (12.63–19.11 μm). Three sample types — bare Ti-6Al-4V alloy, HA Coating Seashell, and HA Coating Commercial — were then machined by conventional drilling and laser trepanning to investigate and compare their machinability characteristics. For conventional drilling, feed rate (0.125 to 0.5 mm/rev) and spindle speed (630 to 1800 rpm) were varied across an L9 Taguchi orthogonal array. For laser trepanning, duty cycle (20–50%), pulse frequency (500–2000 Hz), and trepanning speed (0.05–0.18 mm/s) were varied across an L9 array. Hole diameter, taper angle, and material removal rate (MRR) were measured as response variables. The main effect plots revealed that spindle speed is the dominant parameter for hole diameter and taper angle in conventional drilling, while feed rate dominates MRR. In laser drilling, duty cycle was the most influential parameter for hole diameter and taper angle, while trepanning speed dominated MRR. HA-coated samples exhibited larger hole diameters and significantly higher taper angles compared to uncoated Ti-6Al-4V due to brittle fracture and delamination behavior of the ceramic coating. Multi-response optimization was carried out using Weighted Grey Relational Analysis (WGRA) combined with the Taguchi method, with a uniform weight distribution of 0.44 for Average Hole Diameter, 0.36 for Taper Angle, and 0.20 for MRR applied across all three materials, reflecting the priority of dimensional accuracy and geometric precision over productivity. The optimal parameters were identified as: Feed = 0.125 mm/rev, Speed = 1800 rpm (A1B3) for all conventional drilling cases, and DC = 20%, Freq = 1000 Hz, Speed = 0.18 mm/s (A1B2C3) for uncoated laser drilling, DC =

20%, Freq = 2000 Hz, Speed = 0.18 mm/s (A1B3C3) for HA Coating Seashell laser drilling, while HA Coating Commercial laser drilling optimal was DC = 20%, Freq = 500 Hz, Speed = 0.18 mm/s (A1B1C3). Analysis of Variance (ANOVA) confirmed that for uncoated conventional drilling, feed rate (43.91%) and spindle speed (47.74%) contributed nearly equally, with both statistically significant ($P < 0.05$). For HA Coating Seashell conventional drilling, spindle speed was the dominant factor contributing 85.96% ($P = 0.0039$). For uncoated laser drilling, duty cycle contributed 76.47% ($P = 0.0213$). For HA Coating Seashell laser drilling, duty cycle (43.08%), trepanning speed (31.48%), and frequency (22.29%) shared influence more evenly. For HA Coating Commercial conventional drilling, speed contributed 73.00% ($P = 0.0209$), while for HA Coating Commercial Laser Drilling, duty cycle contributed 42.64%. This study establishes baseline machinability data for flame-sprayed biogenic and commercial HA coatings and identifies the process parameters that govern hole quality. The comparison between seashell-derived and commercial HA coatings provides insight into the effect of HA powder source on machinability. The findings provide a foundation for optimizing drilling and laser processing of HA-coated biomedical implants for clinical applications.

Keywords: Hydroxyapatite, Ti-6Al-4V, Flame Spraying, Conventional Drilling, Laser Trepanning, Grey Relational Analysis, Taguchi, ANOVA, Machinability, Biogenic Coating, Commercial Coating

TABLE OF CONTENTS

LIST OF FIGURES ..... **x**

LIST OF TABLES ..... **xiii**

NOMENCLATURE ..... **xv**

CHAPTER 1: INTRODUCTION AND LITERATURE REVIEW **1**

1.1 Introduction 1

1.2 Literature Review 7

1.3 Research Gaps 10

1.4 Research Objectives 10

1.5 Organization of the Thesis 11

CHAPTER 2: MATERIALS AND METHODOLOGY **12**

2.1 Substrate Preparation 12

2.2 Deposition of HA Coatings 13

2.3 Machining of HA Coatings 15

2.3.1 Conventional Drilling 15

2.3.2 Laser Trepanning 17

2.3.3 Sand Blasting 18

2.4 Characterization and Measurement Methods 20

2.5 Taguchi Experimental Design and S/N Ratios 21

2.6 Multi-response Optimization: Grey Relational Analysis (GRA) 21

2.7 Analysis of Variance (ANOVA) 22

CHAPTER 3: RESULTS AND DISCUSSION **24**

3.1 Surface Roughness and Thickness of As-Deposited Coatings 24

3.2 Blasting Characterization Results 26

3.3 Conventional Drilling: Effect of Parameters on Hole Diameter....27
3.4 Conventional Drilling: Effect of Parameters on MRR....29
3.5 Conventional Drilling: Effect of Parameters on Taper Angle....30
3.6 Laser Drilling: Effect of Parameters on Hole Diameter....32
3.7 Laser Drilling: Effect of Parameters on MRR....35
3.8 Laser Drilling: Effect of Parameters on Taper Angle....37
3.9 Surface Roughness of Drilled Holes....39

CHAPTER 4: OPTIMIZATION USING TAGUCHI S/N RATIO METHOD....41
4.1 Main Effects: Conventional Drilling of Uncoated Samples....41
4.2 Main Effects: Conventional Drilling of HA Coating Seashell Samples....43
4.3 Main Effects: Laser Drilling of Uncoated Samples....44
4.4 Main Effects: Laser Drilling of HA Coating Seashell Samples....46

CHAPTER 5: MULTI-RESPONSE OPTIMIZATION: GRA AND ANOVA....50
5.1 Conventional Drilling of Uncoated Samples....50
5.2 Conventional Drilling of HA Coating Seashell Samples....51
5.3 Laser Drilling of Uncoated Samples....52
5.4 Laser Drilling of HA Coating Seashell Samples....54
5.5 Conventional Drilling of HA Coating Commercial Samples....55
5.6 Laser Drilling of HA Coating Commercial Samples....56
5.7 Optimal Drilling Parameters Summary....57

CHAPTER 6: CONCLUSIONS AND FUTURE SCOPE....59
6.1 Conclusions....59
6.2 Future Scope....61

REFERENCES....62

LIST OF FIGURES

Figure 1.1 Cell growth in simulated body fluid (SBF) 1
Figure 1.2 Conventional drilling setup and samples 2
Figure 1.3 Laser drilling setup and samples 3
Figure 1.4 Ti-6Al-5V knee implant 4
Figure 2.1 Ti-6Al-4V substrate sample. 13
Figure 2.2 Grit blasting suction unit. 13
Figure 2.3 SEM image of HA powder. 14
Figure 2.4 Flame spray setup. 15
Figure 2.5 Conventional drilled hole. 16
Figure 2.6 Schematic representation of conventional drilling processes. 17
Figure 2.7 Laser drilled hole. 18
Figure 2.8 Schematic representation of laser trepanning process. 18
Figure 2.9 Blasted HA coating sample. 19
Figure 2.10 Stylus profilometer and stereo microscope. 20
Figure 3.1 Variation of coating thickness with standoff distance (SOD). 25
Figure 3.2 Variation of surface roughness with standoff distance (SOD). 25
Figure 3.3 Optical microscopy cross-sections of HA coatings at SOD of 70, 90 and 110 mm showing coating-substrate interface and measured thickness values. 25
Figure 3.4 Variation of HA coating surface roughness with blasting time. 26
Figure 3.5 Variation of residual HA coating thickness with blasting time. 27
Figure 3.6 Variation of material removal rate (MRR) with blasting time. 27
Figure 3.7 Variation of average hole diameter with feed rate for conventional drilling 28
Figure 3.8 Variation of average hole diameter with spindle speed for conventional drilling 29
Figure 3.9 Variation of MRR with feed rate for conventional drilling 30
Figure 3.10 Variation of MRR with spindle speed for conventional drilling 30
Figure 3.11 Variation of taper angle with feed rate for conventional drilling 31
Figure 3.12 Variation of taper angle with spindle speed for conventional drilling 32
Figure 3.13 Variation of average hole diameter with duty cycle for laser drilling 33

Figure 3.14 Variation of average hole diameter with pulse frequency for laser drilling.....34
Figure 3.15 Variation of average hole diameter with trepanning speed for laser drilling.....35
Figure 3.16 Variation of MRR with duty cycle for laser drilling 36
Figure 3.17 Variation of MRR with pulse frequency for laser drilling 36
Figure 3.18 Variation of MRR with trepanning speed for laser drilling 37
Figure 3.19 Variation of taper angle with duty cycle for laser drilling 38
Figure 3.20 Variation of taper angle with pulse frequency for laser drilling 38
Figure 3.21 Variation of taper angle with trepanning speed for laser drilling.....39
Figure 3.22 Comparison of inner hole surface roughness for conventional and laser drilled holes. 40
Figure 4.1 Main effect plot for (a) average diameter, (b) MRR, and (c) taper angle of the holes in uncoated samples (conventional drilling).....42
Figure 4.2 Main effect plot for (a) average diameter, (b) MRR, and (c) taper angle of the holes in HA Coating Seashell samples (conventional drilling). 43
Figure 4.3 Main effect plot for (a) average diameter, (b) MRR, and (c) taper angle of the holes in uncoated samples (laser drilling).....45
Figure 4.4 Main effect plot for (a) average diameter, (b) MRR, and (c) taper angle of the holes in HA Coating Seashell samples (laser drilling). 47
Figure 5.1 ANOVA contribution: (a) uncoated and (b) HA Coating Seashell — conventional drilling.....52
Figure 5.2 ANOVA contribution: (a) uncoated and (b) HA Coating Seashell — laser drilling.55
Figure 5.3 ANOVA contribution of HA Coating Commercial: (a) Conventional and (b) laser drilling.....57

LIST OF TABLES

Table 2.1 Elemental composition of Ti-6Al-4V ELI alloy substrate.....12
Table 2.2 Grit blasting parameters.....12
Table 2.3 Ti-6Al-4V substrate preparation specifications.....13
Table 2.4 HA powder properties.....14
Table 2.5 Elemental composition of synthesized HA powder.....14
Table 2.6 Flame spraying deposition parameters. 14
Table 2.7 Preheating parameters.....15
Table 2.8 Conventional drilling setup.....16
Table 2.9 Conventional drilling parameters (varied).....16
Table 2.10 Fixed laser drilling parameters. 17
Table 2.11 Varied laser drilling parameters.....18
Table 2.12 Blasting equipment setup.....19
Table 2.13 Blasting process parameters.....19
Table 2.14 Blasting characterization measurement methods.....20
Table 2.15 Characterization parameters and measurement methods.....21
Table 2.16 Taguchi S/N ratio formulas.....21
Table 3.1 Surface roughness and thickness of HA coatings at different standoff distances. ...24
Table 4.1 Results of uncoated conventional drilling and their corresponding calculated S/N ratios.....42
Table 4.2 Results of HA Coating Seashell conventional drilling and their corresponding calculated S/N ratios. 44
Table 4.3 Results of uncoated laser drilling and their corresponding calculated S/N ratios. ...46
Table 4.4 Results of HA Coating Seashell laser drilling and their corresponding calculated S/N ratios. 48
Table 4.5 Optimal combinations of parameters obtained by S/N ratio analysis.....48
Table 5.1 Reference and deviation sequences after data pre-processing for uncoated conventional drilling. 50
Table 5.2 GRC and WGRG with S/N ratios (uncoated, conventional). 50

Table 5.3 Response table of WGRGs (uncoated, conventional). 51
Table 5.4 ANOVA for WGRG (uncoated, conventional). 51
Table 5.5 GRC and WGRG with S/N ratios (HA Coating Seashell, conventional). 51
Table 5.6 Response table of WGRGs (HA Coating Seashell, conventional). 52
Table 5.7 ANOVA for WGRG (HA Coating Seashell, conventional). 52
Table 5.8 GRC and WGRG with S/N ratios (uncoated, laser). 52
Table 5.9 Response table of WGRGs (uncoated, laser).....53
Table 5.10 ANOVA for WGRG (uncoated, laser). 53
Table 5.11 GRC and WGRG with S/N ratios (HA Coating Seashell, laser). 54
Table 5.12 Response table of WGRGs (HA Coating Seashell, laser). 54
Table 5.13 ANOVA for WGRG (HA Coating Seashell, laser). 54
Table 5.14 GRC and WGRG with S/N ratios (HA Coating Commercial, conventional). 55
Table 5.15 Response table of WGRGs (HA Coating Commercial, conventional).....55
Table 5.16 ANOVA for WGRG (HA Coating Commercial, conventional).....56
Table 5.17 GRC and WGRG with S/N ratios (HA Coating Commercial, laser).....56
Table 5.18 Response table of WGRGs (HA Coating Commercial, laser).....56
Table 5.19 ANOVA for WGRG (HA Coating Commercial, laser).....57
Table 5.20 Optimal drilling parameters after Taguchi WGRG multi-objective optimization..57

NOMENCLATURE

Symbol/Abbreviation	Description
HA	Hydroxyapatite
Ti-6Al-4V	Titanium alloy (Grade 5)
MRR	Material Removal Rate
S/N	Signal-to-Noise Ratio
GRA	Grey Relational Analysis
GRC	Grey Relational Coefficient
GRG	Grey Relational Grade
WGRG	Weighted Grey Relational Grade
ANOVA	Analysis of Variance
SOD	Standoff Distance
DC	Duty Cycle
Ra	Average Surface Roughness
D	Top hole diameter (mm)
d	Bottom hole diameter (mm)
T	Specimen thickness (mm)
f	Feed rate (mm/rev)
N	Spindle speed (rpm)
LBM	Laser Beam Machining
EDS	Energy Dispersive Spectroscopy
SEM	Scanning Electron Microscopy
EDM	Electric Discharge Machining
WC	Tungsten Carbide

CHAPTER 1

INTRODUCTION AND LITERATURE REVIEW

1.1 Introduction

There is an increasing demand for implants, having good quality and long life. On many occasions Ti-6Al-4V material is used as an implant material considering its bio-inert and excellent mechanical properties. However, it has some limitations such as lack of bioactivity and releasing toxic Al^{3+} ions to the body fluid. A suitable coating material such as Hydroxyapatite (HA) on the Ti-6Al-4V surface can not only act as a barrier coating but also be able to provide high bio-activity property [27, 28]. HA is an ideal material for the implants due to its chemical and crystallographic properties that are similar to the mineral components of bones and hard tissue in mammals [29]. In addition, HA promotes the self-healing of bones and is also used as a bone filler material due to its excellent biocompatibility, bioactivity and osteoconductive properties [30]. In general, thermally sprayed HA coatings are deposited on Ti-6Al-4V alloys for the implants such as hip joints, knee joints, and dental implants to enhance their osteointegration [31]. Among various types of HA, the biogenic-derived HA shows higher biological properties than the commercial one due to the presence of trace elements in such material that are beneficial in terms of cell growth in human body [32].

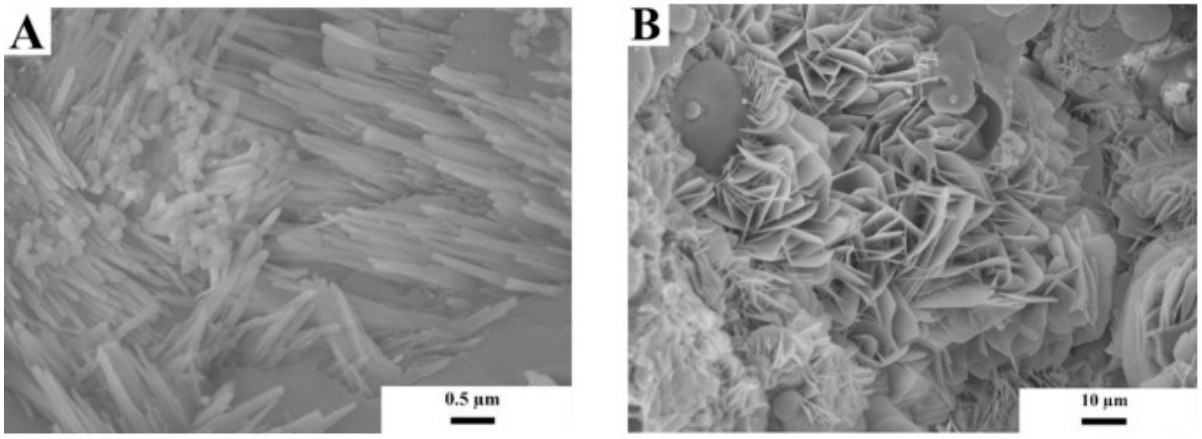


Figure 1.1 Cell growth in simulated body fluid (SBF) [31].

Bio ceramic-based HA coating often requires post-processing to implement these coatings to obtain a shape, size, and surface finish matching the specific requirements of a

patient [5]. In particular, drilling precise holes in coated implants is critical for achieving mechanical fixation through screws and bolts, and also for facilitating easy removal of the implant from the body when required. Therefore, the present research is conducted to optimize the drilling parameters for producing holes with perfect tolerance geometry in HA-coated Ti-6Al-4V substrates, thereby ensuring reliable mechanical fixation and convenient implant retrieval. Machining is one of the post-processing techniques which can give a desired shape useful for the installation of bolts and medical needles in the implants [6]. There are various machining techniques such as electric discharge machining (EDM), laser drilling, and conventional drilling which can be used to produce the hole in the coated implants. However, EDM process is not suitable for electrically non-conductive ceramic-based coating materials. On the other hand, laser processing exhibits high processing efficiency, less processing time, and a wide range of applicable materials such as metals, composites, polymers, and ceramics [1]. Conventional drilling in HA Coating Seashell Ti-6Al-4V specimen may enable customized bioactive implants and support advanced biomedical device applications. However, conventional drilling process is used extensively in manufacturing industries for the enhancement of material removal rate, surface finishing, and productivity of the components using suitable parameters. In conventional drilling, feed rate and speed are identified as key parameters affecting the performance [2].



Figure 1.2 (a). Conventional drilling setup and samples

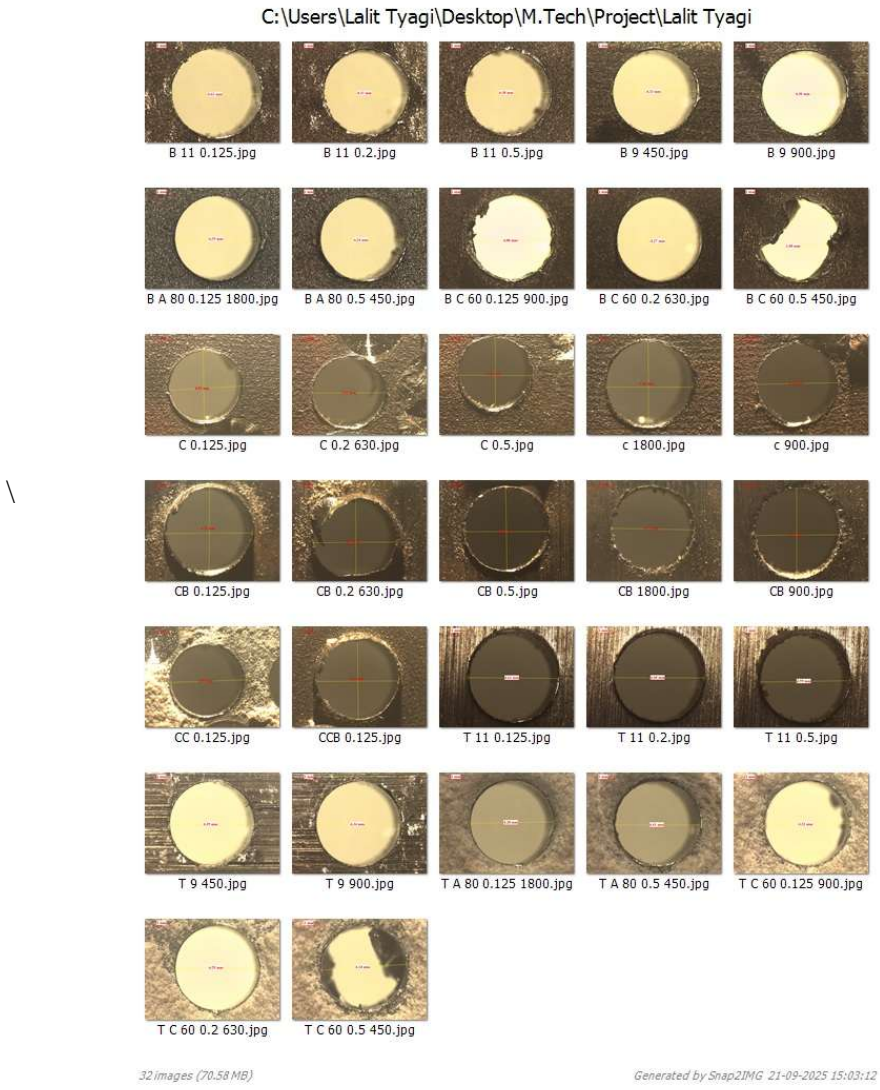


Figure 1.2 (b). Conventional drilling samples

However, some of the features restrict their use in certain applications, such as inclined holes on coated samples. Also, being extremely hard in nature, the HA Coating Seashell implant is often found to be difficult to machine by conventional route such as drilling. To mitigate such issues, laser trepanning would be an alternative option to machine the HA Coating Seashell implants. Laser drilling is preferred over the conventional drilling particularly for fragile bio ceramics, as it prevents the induction of fractures, generation of dust and debris, and introduction of contamination [3]. Several studies have demonstrated laser drilling of biomaterial performed by pulsed femtosecond lasers [4, 13, 14]. Among the beam controlling mechanisms utilized, spiral laser trepanning involves the laser beam gradually removing well-defined geometries [15, 16].



Figure 1.3 (a). Laser drilling samples



Figure 1.3 (b). Laser drilling setup

In this study, three sample types are investigated: bare Ti-6Al-4V alloy (uncoated), seashell-derived HA coating (HA Coating Seashell), and commercial HA coating (HA Coating Commercial). The comparison between biogenic and commercial HA coatings provides insight into the effect of HA powder source on machinability characteristics. Surface coating technology plays a pivotal role in enhancing the performance and longevity of engineering components across diverse industries, including aerospace, automotive, energy, and biomedical sectors. Thermal spray techniques — encompassing plasma spraying, high-velocity oxy-fuel (HVOF) spraying, flame spraying, and cold spraying — are among the most versatile and widely adopted coating deposition methods. These processes accelerate feedstock material (in powder, wire, or rod form) through a high-temperature, high-velocity gas stream onto a prepared substrate, forming a mechanically bonded lamellar coating. Flame spraying, in particular, offers advantages of lower equipment cost, operational simplicity, and the ability to deposit a wide range of ceramic, metallic, and composite coatings. In the biomedical domain, surface coatings serve the critical function of imparting bioactivity, corrosion protection, and wear resistance to metallic implant substrates that would otherwise lack these properties. The quality of the deposited coating — including its thickness, porosity, adhesion strength, phase composition, and surface roughness — is strongly influenced by spray parameters such as standoff distance (SOD), powder feed rate, gas flow rates, and substrate preheating conditions.

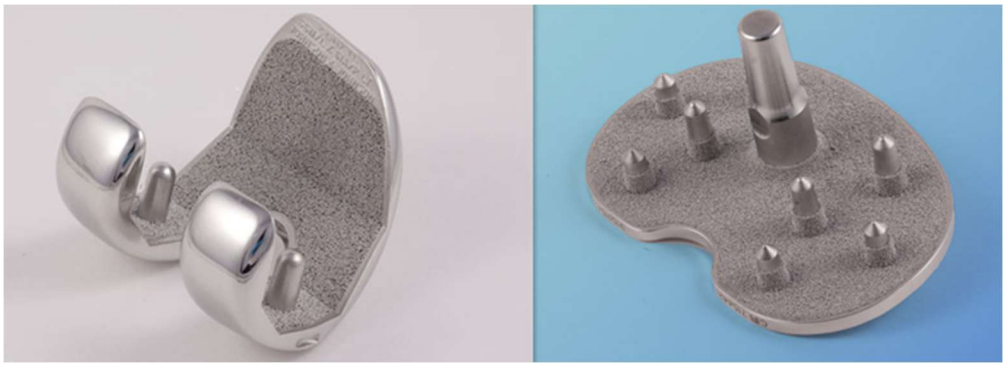


Figure 1.4 Ti-6Al-4V knee implant [42].

The global demand for biomedical implants has grown significantly due to increasing life expectancy, rising prevalence of musculoskeletal disorders, and advances in surgical techniques. Orthopedic and dental implants must satisfy stringent requirements including biocompatibility, adequate mechanical strength, corrosion resistance, and the ability to promote osseointegration — the direct structural and functional connection between living

bone and the implant surface. Metallic biomaterials such as stainless steel (316L), cobalt-chromium alloys, and titanium alloys form the structural backbone of most load-bearing implants. Among these, titanium and its alloys, particularly Ti-6Al-4V, have emerged as the material of choice due to their superior biocompatibility and mechanical properties. However, the bio-inert nature of metallic surfaces necessitates surface modification strategies to enhance biological fixation. The application of bioactive ceramic coatings, especially hydroxyapatite (HA), on metallic substrates represents a well-established approach to bridge the gap between mechanical performance and biological functionality.

Ti-6Al-4V (Grade 5) is the most widely used titanium alloy in biomedical applications, accounting for over 50% of all titanium alloys consumed globally. Its popularity stems from an exceptional combination of high specific strength (strength-to-weight ratio), excellent corrosion resistance in physiological environments, low elastic modulus relative to stainless steels and cobalt-chromium alloys (reducing stress shielding), and proven biocompatibility. The alloy exhibits a two-phase ($\alpha+\beta$) microstructure that can be tailored through thermomechanical processing to optimize mechanical properties. However, Ti-6Al-4V is inherently bio-inert — it does not form a direct chemical bond with bone tissue, which can lead to fibrous encapsulation and eventual implant loosening. Additionally, concerns about the long-term release of toxic Al^{3+} and V^{5+} ions into surrounding tissues have motivated the development of bioactive surface modifications, particularly HA coatings, to combine the structural advantages of Ti-6Al-4V with the biological performance of calcium phosphate ceramics.

Hydroxyapatite (HA), with the chemical formula $Ca_{10}(PO_4)_6(OH)_2$, is the primary inorganic mineral constituent of natural bone and teeth, accounting for approximately 70% of the mineral phase of human bone. Its chemical and crystallographic similarity to biological apatite endows it with excellent bioactivity, osteoconductivity, and the ability to form a direct chemical bond with living bone tissue — a property known as osseointegration. HA coatings on metallic implants significantly enhance early bone apposition and long-term fixation stability. HA can be sourced commercially through chemical synthesis or derived from natural biogenic sources such as bovine bone, fish scales, eggshells, and seashells. Biogenic HA, particularly that derived from Indian clam seashells via the hydrothermal method, has attracted attention due to its trace element composition (Mg, Na, Sr) that closely mimics natural bone mineral, potentially offering superior biological response compared to stoichiometric commercial HA. The comparison between biogenic and commercial HA coatings in terms of their machinability characteristics remains largely unexplored.

Machining of HA-coated implants presents unique challenges due to the brittle nature of the ceramic coating and the ductile metallic substrate beneath it. Post-deposition machining is often necessary to achieve precise dimensional accuracy, surface finish, and geometric features required for patient-specific implant fitment. Conventional drilling using tungsten carbide or high-speed steel tools is widely adopted; however, the abrasive nature of HA leads to rapid tool wear, coating chipping, and delamination at the coating-substrate interface. To overcome these limitations, non-conventional techniques such as laser trepanning have emerged as viable alternatives. Laser trepanning offers contact-free material removal, eliminates tool wear, and can process hard ceramic coatings without mechanical force. However, the thermal nature of laser processing can introduce heat-affected zones (HAZ), recast layers, and micro-cracking. The selection and optimization of machining parameters — whether feed rate and spindle speed for conventional drilling, or duty cycle, pulse frequency, and trepanning speed for laser drilling — are critical in balancing hole quality, dimensional accuracy, and production efficiency. Taguchi experimental design combined with Grey Relational Analysis (GRA) provides a systematic framework for optimizing these multi-response machining characteristics.

1.2 Literature Review

The machining of titanium alloys and bio-ceramic coatings has been extensively investigated using both conventional and non-conventional techniques. Tsai and Chen [1] demonstrated laser shaping of alumina ceramics using Nd:YAG and CO_2 lasers through a fracture machining technique that utilizes groove-crack linkage for material removal, achieving an MRR of approximately 0.15 mm^3/s with surface roughness of about 60 μm. Sharif and Rahim [2] evaluated the performance of coated and uncoated carbide drills during conventional drilling of Ti-6Al-4V and found that TiAlN-coated drills exhibited 24 times longer tool life with surface roughness values of 0.7–1.0 μm, though high cutting speeds led to rapid tool wear. Avvari et al. [3] optimized hole characteristics during pulse Nd: YAG laser drilling of commercially pure titanium (Grade 4), reporting a 16.9% improvement in MRR and 36% reduction in taper angle at optimal conditions of 5 MPa O_2 pressure and 30 m/min cutting speed. Chatterjee et al. [4] conducted an experimental study on CO_2 laser drilling of Ti-6Al-4V and established that laser power dominates hole taper and heat-affected zone (HAZ), with optimal quality achieved at 2250 W power, 40 Pa gas pressure, and 1600 Hz pulse frequency.

Yuan et al. [7] presented a comprehensive review comparing conventional twist drilling, laser drilling, electrical discharge machining (EDM), and rotary ultrasonic machining (RUM) of Ti-6Al-4V, concluding that non-conventional methods produce cleaner holes but may increase cost and taper angle. Vasudevan et al. [6] investigated drilling of yttria-stabilized zirconia (YSZ) thermal barrier coatings on nickel-based superalloys and found that abrasive water jet machining (AWJM) was the most suitable technique for producing cold, defect-free holes, while laser and EDM processes showed thermal cracking. Water-jet guided laser drilling has also been explored for thermal barrier coating/nickel-alloy systems [7], where high-velocity waterjet guides nanosecond laser pulses to produce clean film cooling holes with minimal recast layer and HAZ, making it suitable for large-thickness TBCs.

Several studies have addressed the grinding and machining of thermally sprayed ceramic coatings. Zhang et al. [8] conducted one of the earliest comprehensive studies on grinding of nanostructured Al_2O_3-TiO_2 and WC-Co coatings deposited by atmospheric plasma spraying (APS), establishing baseline grinding parameters for thermal sprayed ceramics. Fluidized bed machining of APS TiO_2/Cr_2O_3/WC-Co coatings [9] demonstrated that abrasive size, jet pressure, and standoff distance control surface finish in fast-regime processing. Material removal mechanisms in alumina coatings via super abrasive grinding [10] were found to involve brittle fracturing, ductile cutting, and pullout mechanisms, with grinding parameters significantly affecting surface integrity. Kar et al. [11] studied six plasma-sprayed ceramic coatings under high-speed grinding conditions and reported that micro-brittle fracture dominates at high speeds, with surface quality improving through optimized wheel speed and depth of cut.

The machinability of hydroxyapatite (HA) ceramics has been investigated through various conventional and ultrasonic machining approaches. Bhattacharya et al. [12] presented a foundational study on HA machinability, identifying key problems of surface integrity retention, micro-cracking, and chipping during drilling of sintered HA ceramics. Majumdar et al. [13] optimized HAp-Yttrium Phosphate (YP) composite for drill ability using both HSS and carbide drills, finding that YP addition improved machinability. Similarly, Bhattacharya et al. [14] drilled β-TCP/YP composites and reported that increasing YP content improved drilling performance and surface quality. Das et al. [15] employed ultrasonic machining (USM) for hard and brittle HA to avoid thermal, electrical, and chemical changes, optimizing parameters for surface quality and material removal rate. Mehar et al. [16] applied Taguchi

mixed-level design on HA-polypropylene (PP) composite plates and found that feed rate is the dominant parameter for MRR, with optimal conditions at 20 vol.% HAp and 2000 rpm speed. In a subsequent study, Mehar et al. [17] used a Taguchi L27 orthogonal array for CNC drilling of HA-polycarbonate/polystyrene composites, optimizing thrust force and surface roughness with inputs of HAp volume fraction, speed, feed, and drill diameter.

Electrical discharge machining with HA powder additives has emerged as a dual-function technique for biomedical applications. HA-mixed EDM [18] has been demonstrated to simultaneously machine and coat metallic biomaterials by adding HA powder to the EDM dielectric fluid, achieving both material removal and surface modification in a single process. Further work on HA-mixed EDM of SS 316L substrates [19] reported a recast layer thickness of 10.74 μm and surface roughness of 2.688 μm, with HA powder concentration affecting both coating quality and machining rate.

Laser-based processing of HA has been explored for various applications including drilling, ablation, and surface modification. Meireles et al. [20] used water-jet guided laser to drill parallel and lateral sub-millimeter channels in biomorphic HA scaffolds, enhancing porosity for cell and fluid infiltration. Katto et al. [21] investigated excimer laser ablation of sintered HA and found that photochemical ablation using ArF and KrF lasers produces flat-bottom holes with sharp edges, while XeF shows photothermal damage, emphasizing the critical importance of wavelength selection for HA processing. Paital et al. [22] demonstrated that excimer laser (KrF) treatment forms rough columnar and cone-shaped surface topography on dense HA, improving cell attachment potential through controlled surface texturing. Um et al. [23] achieved simultaneous synthesis and coating of HAp via nanosecond laser surface treatment, producing robust coatings with enhanced adhesion through a laser-induced hydrothermal process. Ke et al. [40] developed gradient HA coatings on Ti-6Al-4V using LENS™ combined with plasma spraying, where the LENS™ interfacial layer enhanced coating adhesion through a compositionally graded approach. Buser/Benetti group [41] demonstrated that Ti surfaces treated with laser ablation followed by thin HA deposition showed significantly higher cortical bone-to-implant contact (BIC), confirming enhanced osseointegration in vivo. Pecora et al. [26] measured removal torques and found values of 23–34 N.cm for machined surfaces, 33–55 N.cm for laser-modified surfaces, and 55–64 N.cm for HA-coated surfaces, demonstrating that combined laser and HA treatment provides the best biological fixation in a rabbit model.

From the above literature survey, it is evident that while extensive research has been conducted on the machining of titanium alloys and bulk HA ceramics individually, the machinability of HA coatings deposited on metallic substrates remains largely unexplored. In particular, no study has systematically investigated the drilling characteristics of flame-sprayed biogenic (seashell-derived) HA coatings on Ti-6Al-4V using both conventional and laser trepanning processes, nor has the comparison between biogenic and commercial HA coatings in terms of their machinability been reported. This gap motivates the present research work.

1.3 Research Gaps

From the extensive literature review, the following research gaps have been identified:

- Not many works exist on machining of HA coatings deposited on metallic substrates.
- Very few works are available on machinability study of HA Coating Seashell Ti-alloy.
- No work has been reported on the machinability of flame sprayed sea-shell derived HA coating on Ti-6Al-4V substrates.
- The optimization of machining parameters for biogenic HA Coating Seashell Ti-6Al-4V using Taguchi-GRA method has not been explored.

1.4 Research Objectives

The objectives of this research are as follows:

1. To deposit seashell-derived Hydroxyapatite (HA) coating on Ti-6Al-4V substrate using flame spray technique at various standoff distances (SODs) and study the effect of the same on deposited coatings.
2. To investigate and compare the machinability characteristics such as dimensional accuracy, MRR and surface finish of HA coating with that of uncoated Ti-6Al-4V substrate while machining by conventional drilling and laser trepanning processes.
3. To optimize machining parameters by identifying and ranking the key factors affecting machining performance using Taguchi Grey Relational Analysis and ANOVA.
4. Comparison of commercial HA coating deposited on Ti-6Al-4V substrate using flame spray technique with seashell derived HA coatings and optimize their parameters.

1.5 Organization of the Thesis

This thesis is organized into six chapters. Chapter 1 presents the introduction, literature review, research gaps, and objectives. Chapter 2 describes the materials and methodology, including substrate preparation, HA coating deposition, machining processes (conventional drilling, laser trepanning, and sand blasting), characterization methods, Taguchi experimental design, Grey Relational Analysis (GRA), and ANOVA. Chapter 3 presents the results and discussion covering coating characterization, blasting results, and the effect of process parameters on hole diameter, MRR, taper angle, and surface roughness for all three sample types. Chapter 4 discusses the Taguchi S/N ratio optimization for conventional and laser drilling. Chapter 5 presents the multi-response optimization using Weighted Grey Relational Analysis and ANOVA for all six drilling cases (three samples × two processes). Chapter 6 summarizes the conclusions and suggests the scope for future work.

CHAPTER 2

MATERIALS AND METHODOLOGY

2.1 Substrate Preparation

To prepare the specimens, a Ti-6Al-4V (ELI) alloy plate was sectioned into dimensions of (30 × 30 × 3) mm using wire-EDM (Berline CNC Wire Cut) machine. The elemental composition of the Ti-6Al-4V ELI alloy is presented in Table 2.1, confirmed by the EDS analysis. Further, the specimens were blasted with 18 mesh size of Al_2O_3 grits using a suction blaster machine (Synco Industries Ltd., Jodhpur) to create roughness over the surface. Subsequently, blasted specimens were degreased by ultrasonication in acetone bath. Blasting was operated at 100 mm standoff distance (SOD) and 0.5 MPa of air pressure for 30 seconds. The average roughness (Ra) of the blasted surface was obtained as around 5 μm, measured by contact type stylus profilometer (Taylor Hobson). Prior to spraying, blasted specimens were ultrasonically cleaned in acetone using a sonicator bath (Ultrasonic Solutions) to remove the residue of grits and dust particles.

Table 2.1 Elemental composition of Ti-6Al-4V ELI alloy substrate.

Element	**Composition (wt. %)**
Vanadium (V)	3.5–4.5
Aluminum (Al)	5.5–6.5
Titanium (Ti)	Balance (88–91%)

Table 2.2 Grit blasting parameters.

S.N.	**Parameter**	**Value**
1	Media	Alumina grit (18 mesh)
2	Time	95 s
3	Standoff distance	100 mm
4	Blasting pressure	0.5 MPa

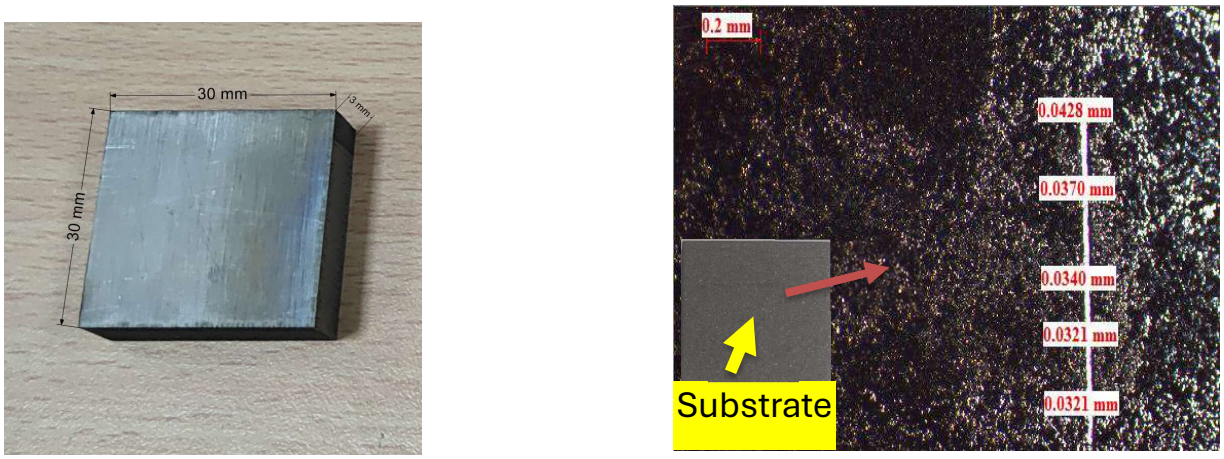


Figure 2.1 Ti6AL4V Sample



Figure 2.2 Grit blasting suction unit

Table 2.3 Ti-6Al-4V substrate preparation specifications.

S.N.	Parameter	Value
1	Substrate dimensions	30 × 30 × 3 mm^3
2	Avg. roughness obtained (Ra)	4–5 µm

2.2 Deposition of HA Coatings

Synthesized hydroxyapatite (HA) powder was used as feedstock material. HA powder was successfully synthesized from Indian clam seashell via the hydrothermal process. The detailed synthesis process of HA powders is explained in previous research [40]. The chemical reaction for the synthesis is:

$CaCO_3 \rightarrow CaO + CO_2\uparrow$

$CaO + 3Ca_3(PO_4)_2 + H_2O \rightarrow Ca_{10}(PO_4)_6(OH)_2$

Table 2.4 HA powder properties.

S.N.	Parameter	Value/Range
1	Heat treatment temperature	800 °C
2	Average particle size	16.59 ± 0.44 µm



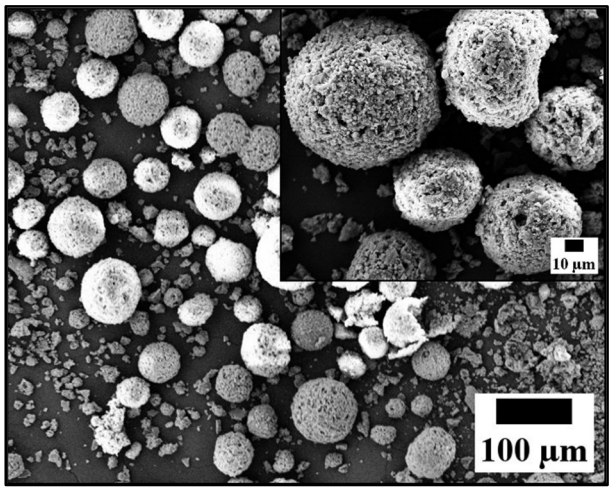


Figure 2.3 SEM image of HA Powder.

Table 2.5 Elemental composition of synthesized HA powder.

S.N.	Element	Weight Percent (%)
1	Calcium (Ca)	~39.7
2	Phosphorus (P)	~18.5
3	Oxygen (O)	~41.0–41.5
4	Hydrogen (H)	~0.2

The HA coatings were deposited by the flame spray technique. A powder jet-86 gun (MEC, Jodhpur) mounted in an X-Y manipulator (Shotblaster, Jodhpur) was employed to spray the feedstock material in linear motion with 30% overlapping of the coating. Prior to deposition, the substrates were pre-heated up to 200 °C using an oxy-acetylene flame. The deposition parameters are listed in Table 2.6

Table 2.6 Flame spraying deposition parameters.

S.N.	Parameter	Value
1	Acetylene gas flow rate	28 l/min
2	Oxygen gas flow rate	34 l/min
3	Acetylene pressure	97 kPa
4	Oxygen pressure	192 kPa

5	Powder feed rate	3 g/min
6	Standoff distance (SOD)	70, 90, 110 mm

Table 2.7 Preheating parameters.

S.N.	Material	Preheating Temperature
1	HA powder	110 °C
2	Ti-6Al-4V substrate	250 °C

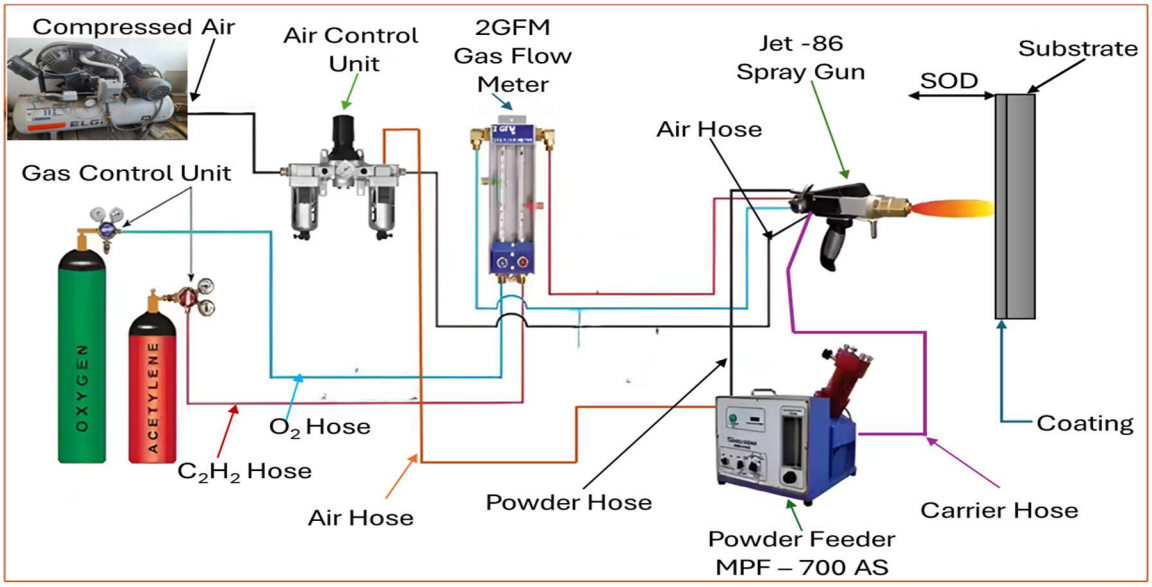


Figure 2.4 Flame Spray Setup

2.3 Machining of HA Coatings

2.3.1 Conventional Drilling

Conventional drilling was employed on the uncoated Ti-6Al-4V plates and HA Coating Seashell samples using a geared radial drilling machine (HMT RM62). Drilling was operated at feed rates of 0.125, 0.2, and 0.5 mm/rev and spindle speeds of 630, 900, and 1800 rpm with a tungsten carbide drill bit of 4 mm diameter. During the process, water-soluble oil mixture served as coolant and was continuously supplied to the drilling zone. Multiple holes were produced for each operating parameter set to maintain result reliability.

Table 2.8 Conventional drilling setup.

S.N.	Equipment	Material/Make	Properties
1	Drilling Machine	HMT-RM62	Geared, Radial
2	Drill Bit	Tungsten Carbide (WC)	Dia = 4 mm, Helix angle = 30°
3	Workpiece	HA Coated & Uncoated Ti-6Al-4V	Substrate = 3 mm, Coating ≈ 300 µm
4	Coolant	Soluble Oil Mixture	Water + Industrial Oil

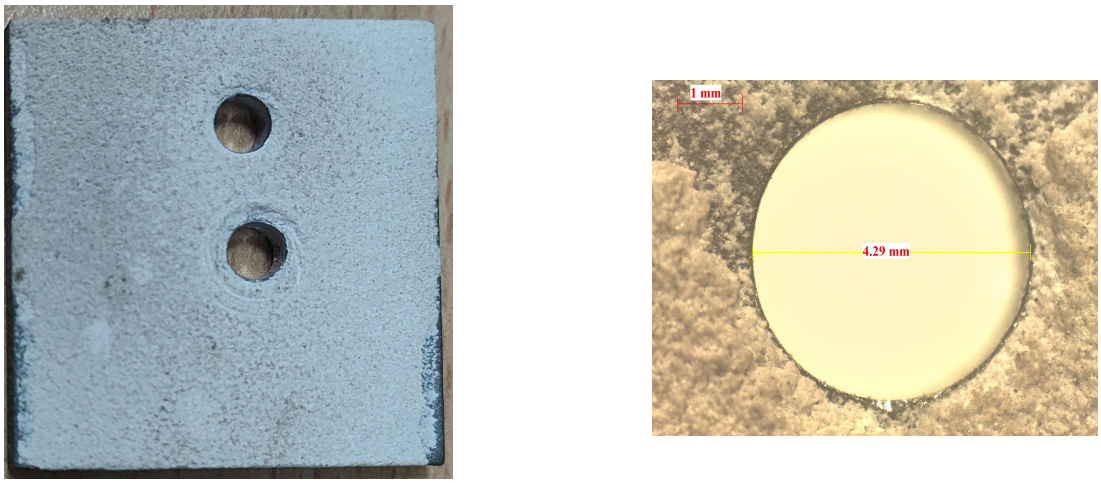


Figure 2.5 Conventional Drilled Hole

Table 2.9 Conventional drilling parameters (varied).

S.N.	Feed Rate (mm/rev)	Spindle Speed (RPM)
1	0.125	630
2	0.2	900
3	0.5	1800

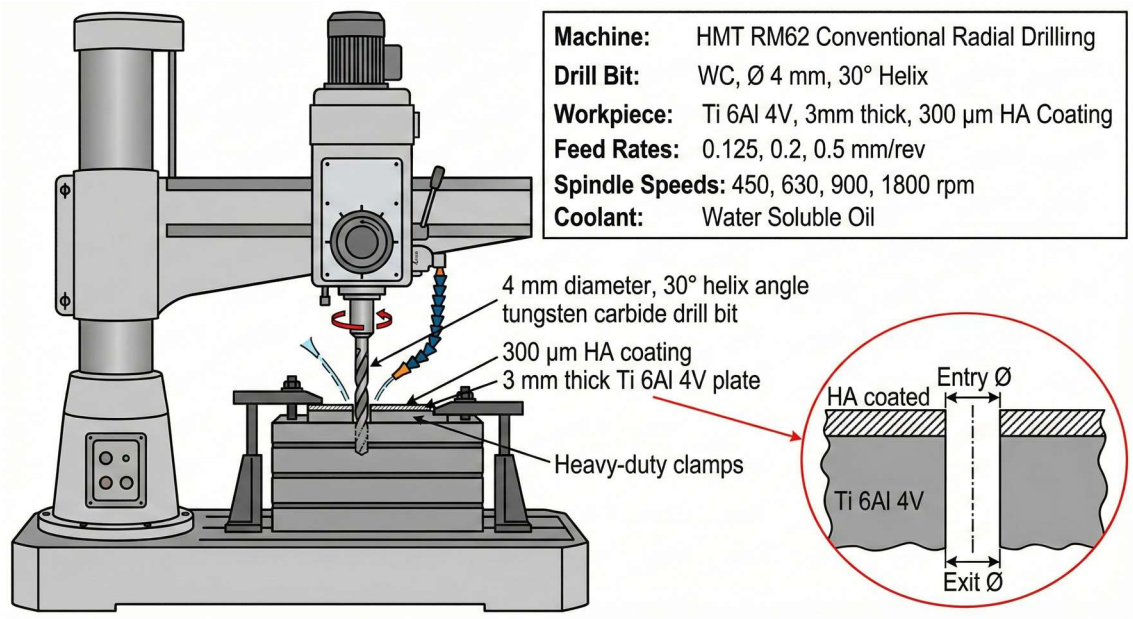


Figure 2.6 Schematic representation of conventional drilling processes.

2.3.2 Laser Trepanning

Laser drilling was performed through trepanning mode on uncoated and HA Coating Seashell samples using a Sparkle 6-axis fiber laser robot system. The laser operated at 1500 W power with 1064 nm wavelength in constant power mode. Argon gas was used as shielding gas to prevent oxidation. The detailed process parameters are listed in Tables 2.10 and 2.11.

Table 2.10 Fixed laser drilling parameters.

S.N.	Parameter	Value
1	Hole/Trepanning Diameter	4 mm
2	Nozzle Diameter	1.6 mm
3	Spot Diameter	0.02 mm
4	Power	1500 W
5	Standoff Distance	50 mm
6	Power Mode	Constant
7	Gas Pressure	4.5–5.5 MPa
8	Wavelength	1064 nm
9	Shielding Gas	Argon (Ar)

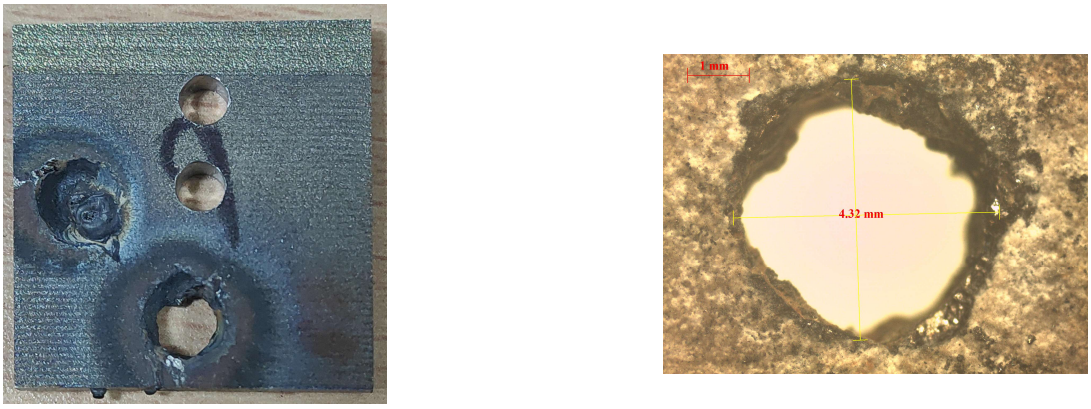


Figure 2.7 Laser Drilled Hole

Table 2.11 Varied laser drilling parameters.

S.N.	Duty Cycle (%)	Frequency (Hz)	Trepanning Speed (mm/s)
1	20	500	0.05
2	35	1000	0.08
3	50	2000	0.18

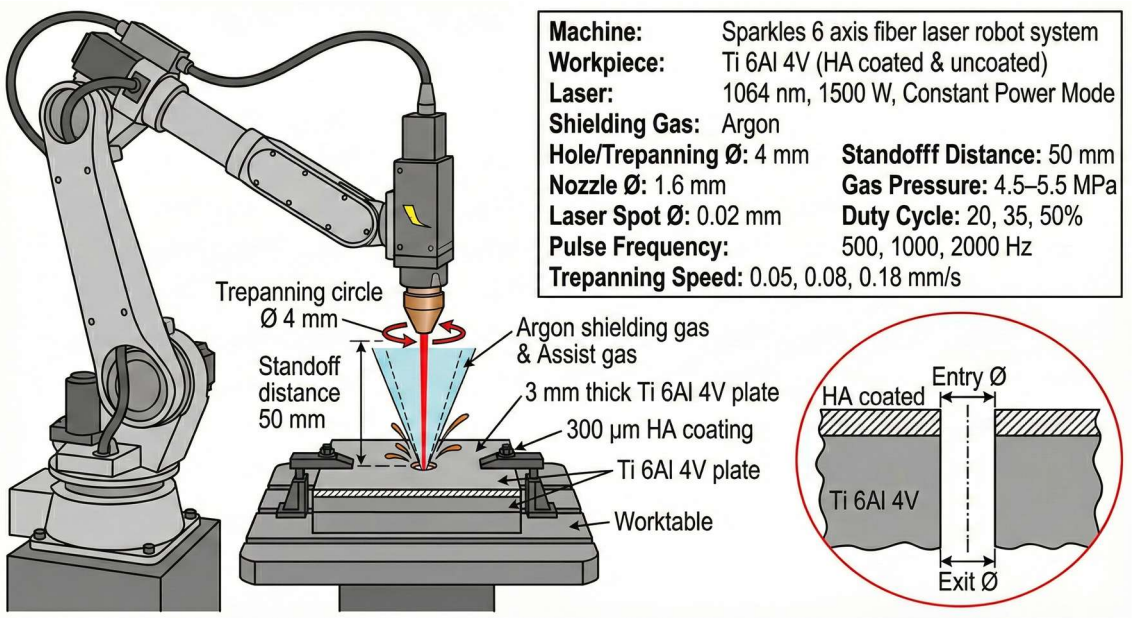


Figure 2.8 Schematic representation of laser trepanning process.

2.3.3 Sand Blasting

In addition to drilling, sand blasting experiments were conducted on HA Coating Seashell Ti-6Al-4V substrates to evaluate the erosion resistance of the coating. The blasting setup and

parameters are summarized in Tables 2.12 and 2.13. Alumina grit (20 mesh) was used as the blasting medium at a pressure of 0.5 MPa with a standoff distance of 170 mm. Three different blasting durations (0.7, 1.13, and 2.05 seconds) were used to assess the material removal rate and coating integrity under erosive conditions.

Table 2.12 Blasting equipment setup.

S.No.	Equipment	Material/Make Model
1	Blasting Machine	Synco Industries 1046
2	Workpiece	HA Coated Ti-6Al-4V Substrate
3	Air Compressor	Elgi SS10LB

Table 2.13 Blasting process parameters.

S.No.	Parameter	Value(s)
1	Media	Alumina grit
2	Grit Size	20 Mesh
3	Time (varying)	0.7, 1.13, 2.05 seconds
4	Standoff Distance	170 mm
5	Blasting Pressure	0.5 MPa

The characterization measurements for blasting experiments were carried out to evaluate the effect of blasting duration on coating roughness, residual thickness, and material removal rate. The measurement equipment and methods used are summarized in Table 2.14

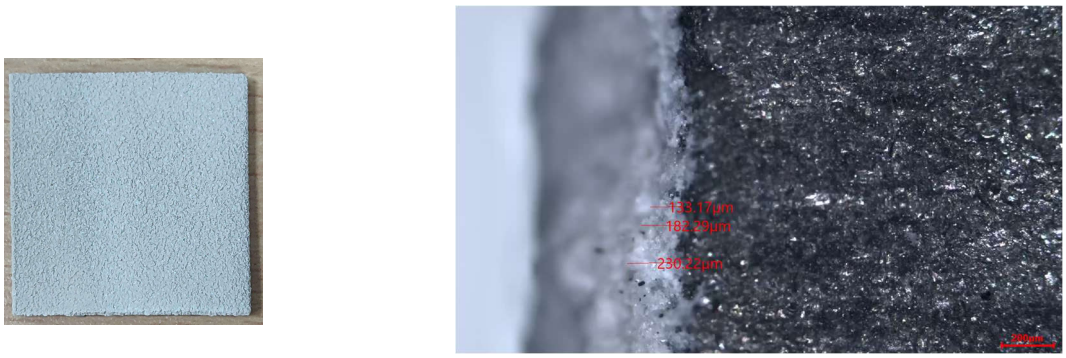


Figure 2.9 Blasted HA Coating Sample

Table 2.14 Blasting characterization measurement methods.

S.No.	Parameter	Equipment/Software	Settings/Method
1	MRR	Mettler Toledo weighing scale ML3202 & Minitab	MRR (mm^3/min) = (W_{aeoxne} − W_{aoxen}) / (ρ × t)
2	Coating Roughness	Stylus Profilometer (Surtronic 25)	Evaluation Length = 4 mm, Gaussian filter
3	Coating Thickness	Olympus upright optical microscope BX53M	50x Darkfield Image Scaling

2.4 Characterization and Measurement Methods

The average diameter of both conventional and laser drilled holes were measured by image analysis technique. Multiple images of both sides of the drilled samples were captured by stereo microscope (Leica EZ4 HD). Further, average diameter was considered as the mean of top and bottom diameter of the drilled samples, measured using Image-J software.

The taper angle of the holes was calculated using the expression:

Taper angle (θ) = $\arctan[(D - d) / 2T]$ ..... (2.1)

where D is top diameter (mm), d is bottom diameter (mm), and T is specimen thickness (mm).

The surface roughness (Ra) of drilled holes was measured using a stylus profilometer (Surtronic 25), with evaluation length of 2.5 mm and cut-off length of 0.8 mm using Gaussian filter.

The material removal rate (MRR) was calculated for both processes:

For conventional drilling: $MRR = (\pi/4) \times d^2 \times f \times N$ ..... (2.2)

For laser drilling: $MRR = (\pi d^2/4) \times (h/t)$ ..... (2.3)

where d is the diameter of the hole (mm), f is the feed rate (mm/rev), N is the rotational speed (rpm), h is the drill depth (mm), and t is the drilling time (s).



Figure 2.10 Stylus Profilometer and Stereo Microscope

Table 2.15 Characterization parameters and measurement methods.

S.N.	Parameter	Equipment/Software	Settings/Method
1	Average Diameter	Stereo microscope (Leica EZ4 HD) & Image-J	5–6 readings of D_top & D_bottom
2	Taper Angle	Minitab (Formula)	$\theta = \arctan(0.5\times(D-d)/T)$
3	MRR	Minitab (Formula)	Equations 2.2 and 2.3
4	Hole Roughness	Stylus Profilometer (Surtronic 25)	Eval. length: 2.50 mm, Cut-off: 0.8 mm

2.5 Taguchi Experimental Design and S/N Ratios

A Taguchi L9 orthogonal array was designed with nine runs to perform the experiments. For conventional drilling, feed rate (A) and spindle speed (B) were assigned to columns (L9, 3^4) with three levels each. For laser drilling, duty cycle (A), frequency (B), and trepanning speed (C) along with columns of (L9, 3^4) and Taguchi array (L9, 3^3) with three levels were considered.

Signal-to-Noise (S/N) ratio was used to optimize the responses. The S/N ratio was calculated according to:

Smaller-the-better: $S/N = -10 \times \log_{10}[(1/n) \times \Sigma(y_i^2)]$ ..... (2.4)

Larger-the-better: $S/N = -10 \times \log_{10}[(1/n) \times \Sigma(1/y_i^2)]$ ..... (2.5)

Table 2.16 Taguchi S/N ratio formulas.

S.N.	S/N Ratio Case	Formula	Usage
1	Smaller-the-better	$S/N = -10\times\log_{10}((1/n)\times\Sigma y_i^2)$	Minimize response
2	Larger-the-better	$S/N = -10\times\log_{10}((1/n)\times\Sigma(1/y_i^2))$	Maximize response
3	Nominal-the-best	$S/N = 10\times\log_{10}(\bar{y}^2/s^2)$	Target value optimization

2.6 Multi-response Optimization: Grey Relational Analysis (GRA)

Taguchi experimental design method is best suitable for single response optimization. However, for multi-response parameter optimization, Grey Relational Analysis (GRA) method was employed. The data pre-processing was performed using:

Smaller-the-better: $Xi^*(k) = [\max yi(k) - yi(k)] / [\max yi(k) - \min yi(k)]$ .... (2.6)

Larger-the-better: $Xi^*(k) = [yi(k) - \min yi(k)] / [\max yi(k) - \min yi(k)]$ .... (2.7)

After normalization, the deviation sequence was calculated:

Deviation sequence $(\Delta_{0i}) = 1 - x_i^*$ ..... (2.8)

The Grey Relational Coefficient (GRC) was determined using:

$\xi_i = (\Delta\min + \zeta\Delta\max) / (\Delta_{0i} + \zeta\Delta\max)$ ..... (2.9)

where ζ is the distinguishing coefficient set to 0.5. The weightage was assigned as: average diameter = 0.4, taper angle = 0.4, and MRR = 0.2. The Weighted Grey Relational Grade (WGRG) was calculated as:

$WGRG = \Sigma(w_k \times \xi_i(k))$ ..... (2.10)

S/N ratio of $GRG = -10 \times \log_{10}(1/GRG^2)$ ..... (2.11)

2.7 Analysis of Variance (ANOVA)

After computing the Weighted Grey Relational Grade (WGRG) for each experimental run using GRA, Analysis of Variance (ANOVA) was performed to determine the statistical significance and percentage contribution of each process parameter to the overall multi-response performance. The following formulas are used to perform one-way ANOVA on the WGRG values obtained from the Taguchi L9 orthogonal array experiment.

Correction Factor (CF):

$CF = N \times \overline{T}^2$ ..... (2.12)

where N = total number of experimental runs (N = 9 for L9 Taguchi design) and $\overline{T}$ = overall mean of all WGRG values.

Total Sum of Squares (SS_T):

$SS_T = \Sigma(WGRG_i)^2 - CF$ ..... (2.13)

where the summation is over all N experimental runs.

Factor Sum of Squares (SS_factor):

$SS_factor = \Sigma[(Level_j\ Sum)^2 / n_j] - CF$ ..... (2.14)

where Level_j Sum = sum of WGRG values at level j and n_j = number of runs at level j (= 3 for L9 design).

Error Sum of Squares (SS_e):

$SS_e = SS_T - SS_A - SS_B - SS_C$ ..... (2.15)

where SS_A, SS_B, and SS_C are the sum of squares for factors A, B, and C respectively.

Degrees of Freedom (DF):

$DF_factor = k - 1$ (where k = number of levels = 3, so DF = 2) ..... (2.16a)

$DF_total = N - 1 = 8$ ..... (2.16b)

$DF_error = DF_total - DF_A - DF_B - DF_C = 8 - 2 - 2 - 2 = 2$ ..... (2.16c)

Mean Square (Adj MS):

$MS = SS / DF$ ..... (2.17)

F-Statistic:

$F = MS_factor / MS_error$ ..... (2.18)

A higher F-value indicates greater influence of that factor on the WGRG.

Percentage Contribution:

$P\% = (SS_factor / SS_T) \times 100\%$ ..... (2.19)

This indicates the relative importance of each process parameter to the overall multi-response quality characteristic.

The ANOVA results are used in conjunction with the S/N ratio analysis of the WGRG to identify the optimal parameter combination and validate the statistical significance of each factor's contribution.

CHAPTER 3

RESULTS AND DISCUSSION

3.1 Surface Roughness and Thickness of As-Deposited Coatings

The surface roughness and thickness of the flame-sprayed HA coatings were measured at three standoff distances (SODs): 70, 90, and 110 mm. Table 3.1 summarizes the measured values. As the SOD increases from 70 mm to 110 mm, the coating thickness decreases from approximately 369 µm to 237 µm, while surface roughness increases from 12.85 µm to 15.375 µm. The decreasing thickness at higher SODs is attributed to the widening of the spray cone, which disperses the powder over a larger area, reducing the deposition density. The increasing roughness is due to partial solidification of spray particles during the longer flight path at higher SODs, leading to incomplete flattening upon impact and a rougher surface morphology. Figures 3.1 and 3.2 show these trends graphically. Microscopic cross-sectional images at all three SODs confirm the decreasing thickness trend and show good mechanical interlocking at the coating-substrate interface due to the grit-blasted surface preparation (Figure 3.3).

Table 3.1 Surface roughness and thickness of HA coatings at different standoff distances.

S.No.	SOD (mm)	Roughness (µm)	Thickness (µm)
1	70	12.85	369.278
2	90	14.15	300.75
3	110	15.375	236.79

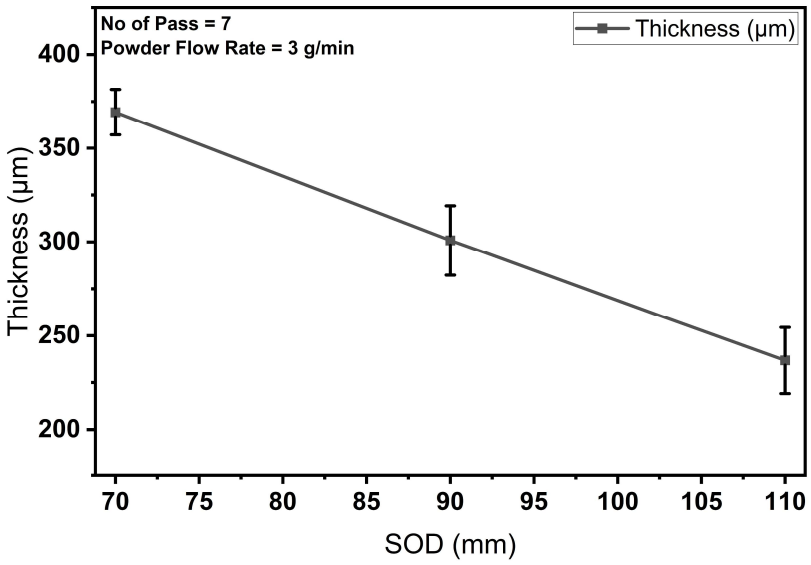


Figure 3.1 Variation of coating thickness with standoff distance (SOD).

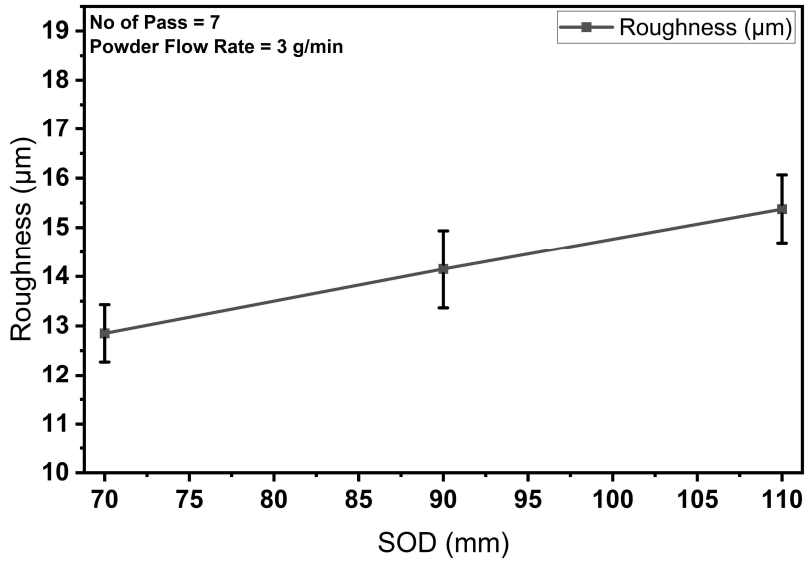


Figure 3.2 Variation of surface roughness with standoff distance (SOD).

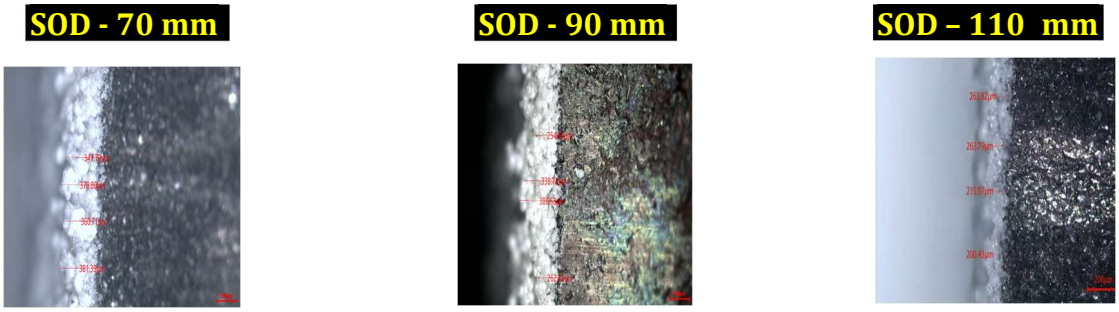


Figure 3.3 Optical microscopy cross-sections of HA coatings at SOD of 70, 90, and 110 mm showing coating-substrate interface and measured thickness values.

3.2 Blasting Characterization Results

The effect of blasting duration on the surface roughness, residual coating thickness, and material removal rate (MRR) of HA-coated Ti-6Al-4V substrates was investigated. Three blasting durations of 0.7, 1.13, and 2.08 seconds were applied using alumina grit (20 mesh) at 0.5 MPa pressure with a standoff distance of 170 mm. Results are presented in Figures 3.4, 3.5, and 3.6.

The roughness increases from approximately 11.8 μm at 0.7 s to about 13.3 μm at 1.13 s, then stabilizes near 13.0 μm at 2.08 s. The initial increase results from mechanical impact of alumina grit particles on the coating surface, creating surface irregularities. The plateau beyond 1.13 s indicates that the roughness saturates, and further blasting does not significantly alter the surface texture.

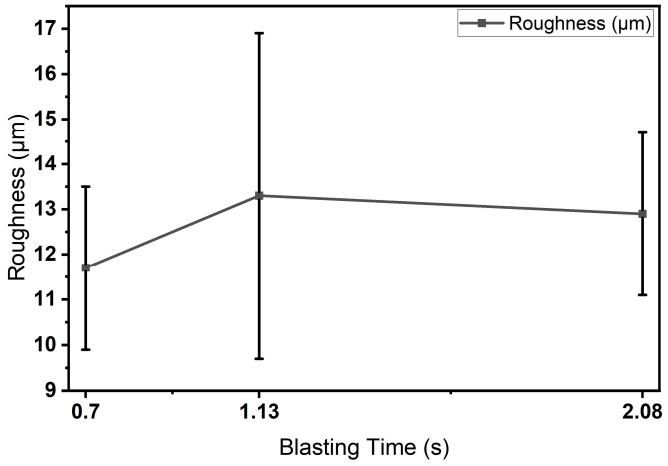


Figure 3.4 Variation of HA coating surface roughness with blasting time.

The thickness decreases significantly from approximately 235 μm at 0.7 s to 125 μm at 1.13 s, and further to approximately 65 μm at 2.08 s. This progressive thinning confirms that abrasive blasting effectively erodes the HA coating. The higher erosion rate at shorter durations slows as the coating becomes thinner and the underlying Ti-6Al-4V substrate, being tougher, offers greater resistance to abrasion.

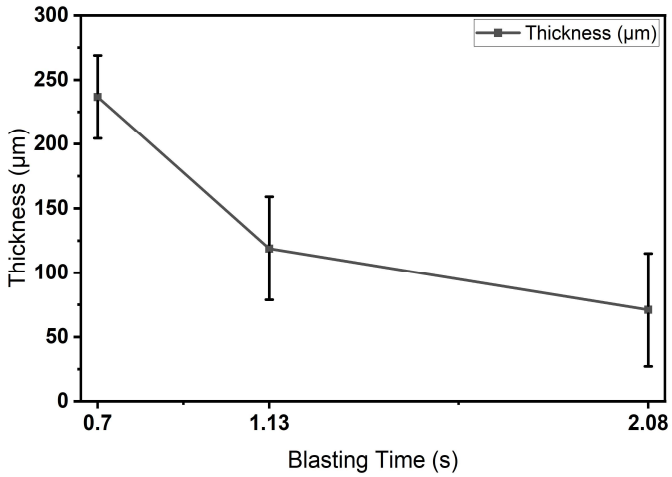


Figure 3.5 Variation of residual HA coating thickness with blasting time.

The MRR remains essentially constant at approximately 0.64–0.65 mm³/min across all three blasting durations, with variations within the experimental error bars. This result indicates that the rate of material removal is independent of blasting duration under the conditions studied, suggesting a stable and uniform erosion mechanism throughout the blasting process.

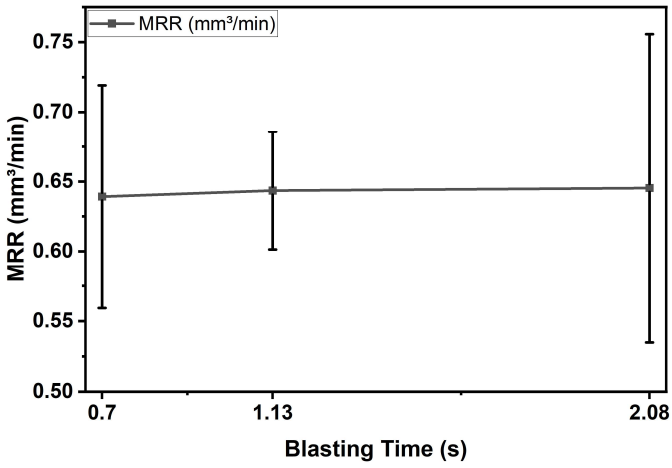


Figure 3.6 Variation of material removal rate (MRR) with blasting time.

3.3 Conventional Drilling: Effect of Parameters on Hole Diameter

In the Taguchi L9 experimental design, all parameters were varied simultaneously across the orthogonal array. The main effect plots present the mean response at each factor level, averaged over all other factor settings. Figure 3.7 shows the main effect of feed rate on the average hole diameter for all three samples. The uncoated Ti-6Al-4V exhibits a slight increase in hole diameter with increasing feed rate, attributed to higher cutting forces causing

drill deflection and elastic recovery of the workpiece material. The HA Coating Seashell shows larger hole diameters compared to uncoated samples across all feed rate levels, owing to brittle fracture and particle detachment at the coating surface during drilling. The HA Coating Commercial exhibits intermediate diameter values, indicating better coating integrity under varying feed conditions. For all three samples, the deviation from the nominal 4 mm diameter increases with feed rate, suggesting that lower feed rates are preferable for dimensional accuracy.

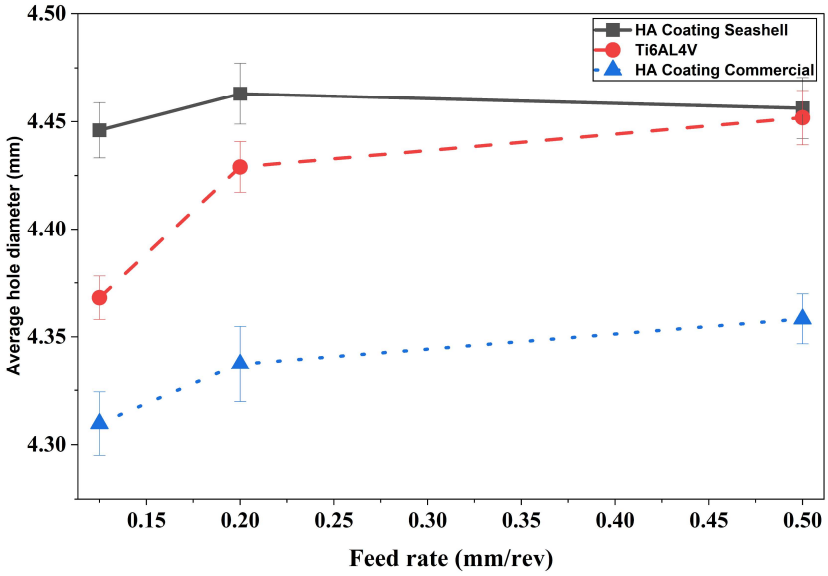


Figure 3.7 Variation of average hole diameter with feed rate for conventional drilling

Figure 3.8 shows the main effect of spindle speed on the average hole diameter for all three samples. The uncoated Ti-6Al-4V exhibits a clear monotonic decrease in hole diameter with increasing spindle speed, indicating improved dimensional accuracy at higher rotational speeds due to better chip evacuation and reduced thrust force. The HA Coating Seashell shows a similar decreasing trend but with consistently larger diameters, reflecting the brittle chipping and delamination behaviour of the ceramic layer during drilling. The HA Coating Commercial follows a comparable trend with diameter values between the uncoated and seashell-coated samples. The main effect plot confirms that spindle speed has a significant influence on hole diameter, with higher speeds producing holes closer to the nominal dimension for all sample types.

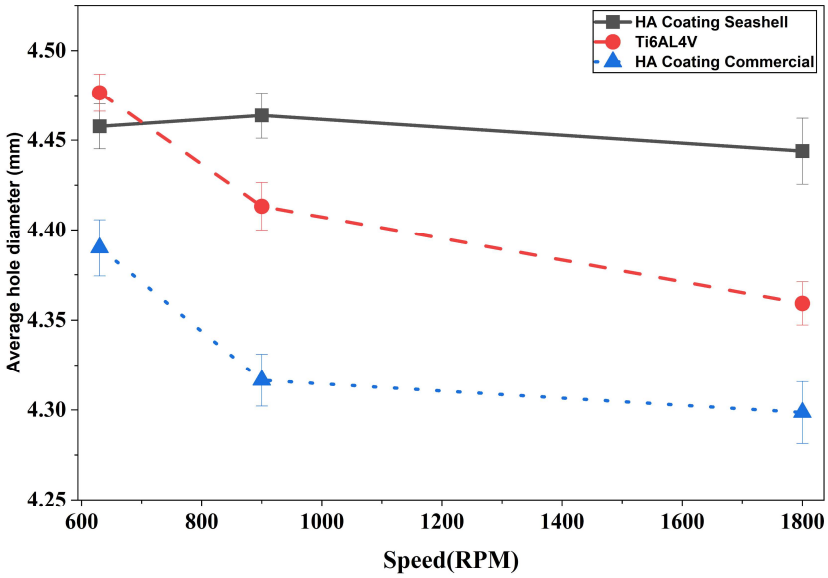


Figure 3.8 Variation of average hole diameter with spindle speed for conventional drilling

3.4 Conventional Drilling: Effect of Parameters on MRR

The main effect plots of feed rate and spindle speed on MRR are presented in Figures 3.9 and 3.10, respectively. Figure 3.9 shows that MRR increases linearly with feed rate for all three sample types, consistent with the drilling MRR formula ($MRR = \pi/4 \times d^2 \times f \times N$). At the highest feed rate level, MRR values reach approximately 700–800 mm^3/min for all samples. The HA Coating Seashell exhibits marginally higher MRR than the uncoated Ti-6Al-4V at equivalent feed rates, attributed to the brittle fracture and particle detachment mechanism in the ceramic coating layer that supplements the cutting action. The HA Coating Commercial shows MRR values comparable to the seashell coating. Figure 3.10 confirms that MRR also increases linearly with spindle speed for all three samples, with uncoated and coated samples showing nearly identical trends. The close agreement in MRR values across all three sample types (within 5% variation) indicates that the presence of the HA coating does not significantly alter the volumetric material removal rate under the parameter ranges studied.

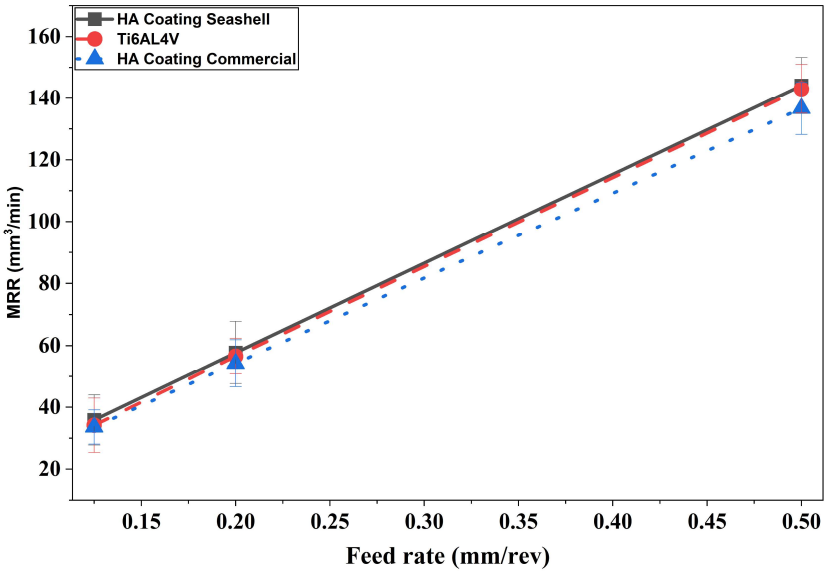


Figure 3.9 Variation of MRR with feed rate for conventional drilling

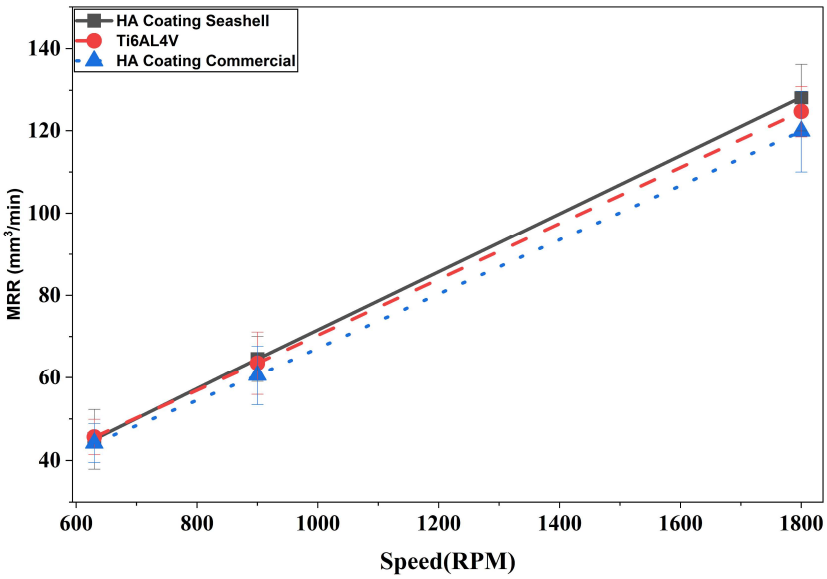


Figure 3.10 Variation of MRR with spindle speed for conventional drilling

3.5 Conventional Drilling: Effect of Parameters on Taper Angle

The main effect of feed rate on taper angle is shown in Figure 3.11 The HA Coating Seashell exhibits dramatically higher taper angles compared to other samples, with taper increasing with feed rate. This is attributed to the brittle nature of the HA coating, which

causes brittle fracture and particle detachment at the hole entry, enlarging the top diameter while the bottom diameter remains relatively unchanged. As feed increases, more material is available at the cutting edge which results in drill deflection and dynamic instability, further increasing the taper angle deviation. The HA Coating Commercial shows intermediate taper values, while the uncoated Ti-6Al-4V exhibits consistently low and stable taper angles across all feed rate levels, owing to the ductile and uniform material removal mechanism in the metallic substrate.

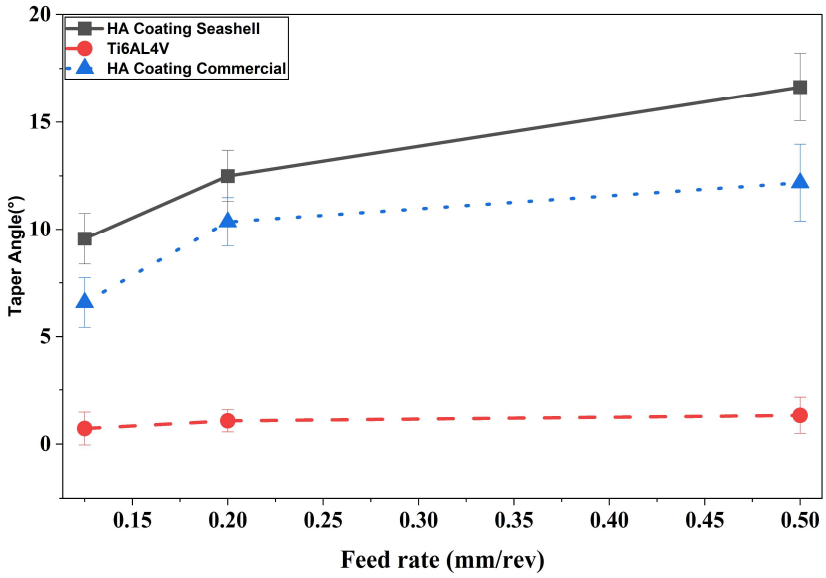


Figure 3.11 Variation of taper angle with feed rate for conventional drilling

Figure 3.12 shows the main effect of spindle speed on taper angle. The HA Coating Seashell exhibits the most dramatic reduction in taper angle with increasing spindle speed, decreasing significantly from low to high speed levels. This behaviour suggests that higher rotational speeds improve the cutting stability and reduce the brittle chipping at the coating surface. The HA Coating Commercial also shows a decreasing trend with speed, while the uncoated Ti-6Al-4V maintains consistently low taper angles across all speed levels. The main effect analysis confirms that spindle speed is the dominant parameter affecting taper angle, particularly for HA-coated samples. Lower feed rate and higher speed produce the minimum deviation of taper angle in both uncoated and HA coated samples, which is preferable for maintaining hole cylindricity.

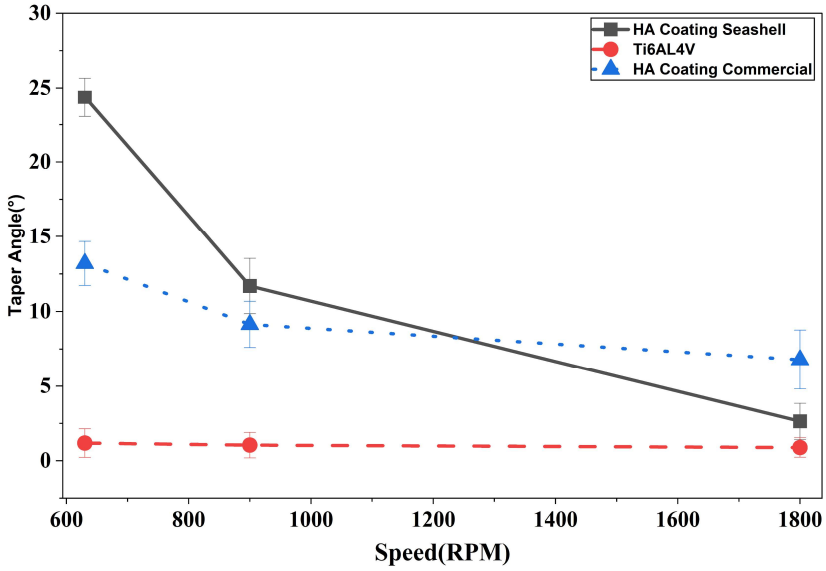


Figure 3.12 Variation of taper angle with spindle speed for conventional drilling

3.6 Laser Drilling: Effect of Parameters on Hole Diameter

In the laser trepanning process, incomplete melt expulsion affects the shape and dimension of the holes, making selection of suitable parameters essential. The main effect plots of laser drilling parameters on the average hole diameter are presented in Figures 3.13, 3.14, and 3.15. Figure 3.13 shows the main effect of duty cycle on average hole diameter. The deviation of hole diameter in HA coated samples increases with duty cycle due to higher energy deposition causing excessive melting at the hole entry. The uncoated Ti-6Al-4V shows increasing trends up to the intermediate duty cycle level, beyond which the hole diameter increases more rapidly due to enhanced melt pool formation at elevated energy densities. The HA Coating Seashell shows a moderate increasing trend, while the HA Coating Commercial shows comparable behaviour. At the lowest duty cycle level (20%), all three samples show hole diameters closest to the nominal 4 mm target, confirming that lower duty cycle improves dimensional accuracy.

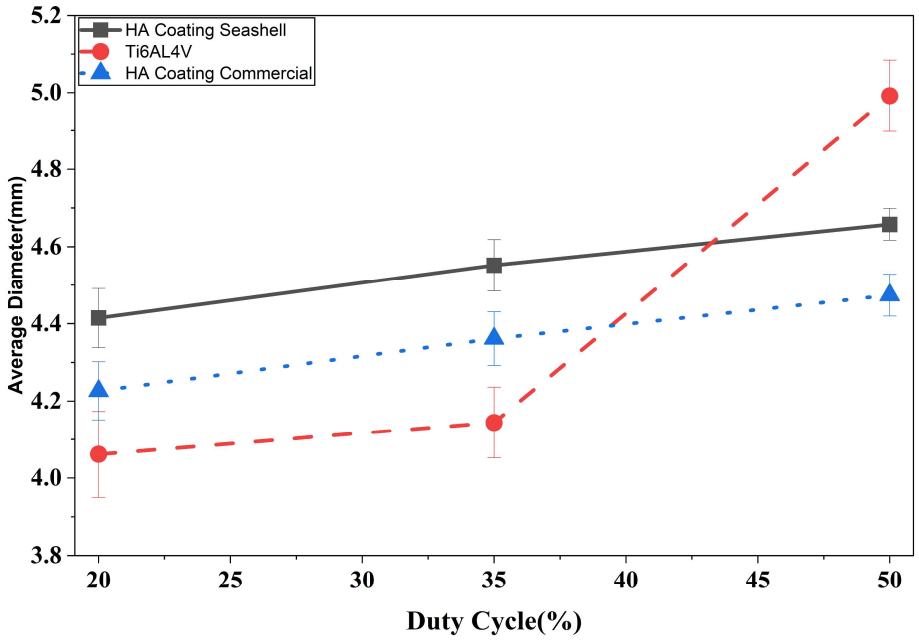


Figure 3.13 Variation of average hole diameter with duty cycle for laser drilling

Figure 3.14 shows the variation of average hole diameter with pulse frequency. All three sample types exhibit a monotonically increasing trend with frequency. The HA Coating Seashell diameter increases from approximately 4.15 mm at 500 Hz to 4.85 mm at 2000 Hz. The uncoated Ti-6Al-4V increases from 4.0 mm to 4.7 mm, and the HA Coating Commercial from 4.1 mm to 4.65 mm. Higher pulse frequencies deliver more laser pulses per unit time, increasing the cumulative thermal energy per pass and consequently enlarging the hole through enhanced ablation. The HA Coating Seashell consistently shows slightly larger diameters than the commercial coating at all frequencies, consistent with the diameter trends observed under duty cycle variation.

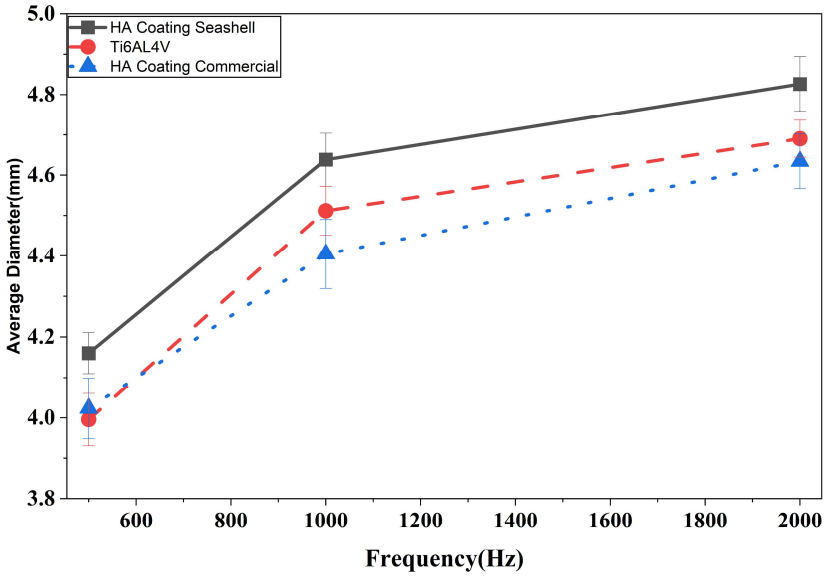


Figure 3.14 Variation of average hole diameter with pulse frequency for laser drilling

Figure 3.15 shows the variation of average hole diameter with trepanning speed. The HA Coating Seashell maintains a nearly constant diameter of approximately 4.55 mm across all trepanning speeds (0.05–0.18 mm/s), indicating that traverse speed has negligible effect on the hole size in this coating. The uncoated Ti-6Al-4V shows a decreasing trend from approximately 4.44 mm at 0.05 mm/s to 4.30 mm at 0.18 mm/s, while the HA Coating Commercial shows a marginal decrease from 4.37 mm to 4.34 mm. The decreasing diameter trend with trepanning speed for uncoated Ti-6Al-4V is due to reduced laser dwell time per unit length at higher traverse speeds, resulting in lower energy deposition per unit area and consequently less material ablation. Among all three laser parameters studied, duty cycle exerts the strongest influence on hole diameter, followed by pulse frequency, with trepanning speed having the least effect.

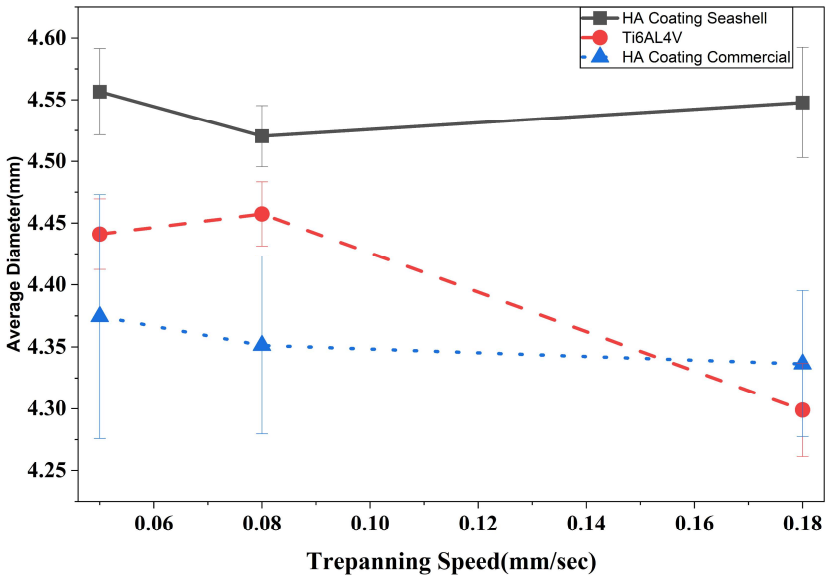


Figure 3.15 Variation of average hole diameter with trepanning speed for laser drilling

3.7 Laser Drilling: Effect of Parameters on MRR

The main effect plots of laser drilling parameters on MRR are shown in Figures 3.16, 3.17, and 3.18. Figure 3.16 shows the main effect of duty cycle on MRR. The uncoated Ti-6Al-4V shows a consistent MRR value up to the intermediate duty cycle level, beyond which it rapidly increases, reflecting higher laser energy causing faster removal rate. The HA Coating Seashell and HA Coating Commercial show relatively stable MRR across duty cycle levels, indicating that the ceramic coatings respond more uniformly to changes in duty cycle. Figure 3.17 shows the main effect of pulse frequency on MRR. The MRR of both uncoated and HA coated samples increases with frequency, primarily due to increased heat accumulation that enhances the efficiency of material melting and vaporization. At lower frequency, the MRR of uncoated and coated samples shows almost similar values. Figure 3.18 illustrates the main effect of trepanning speed on MRR. The MRR linearly increases with trepanning speed for all three sample types, showing the most pronounced effect among all laser parameters. This is due to drilling the hole at shorter duration at higher speeds, leading to higher MRR. Trepanning speed is confirmed as the dominant factor for MRR in laser drilling.

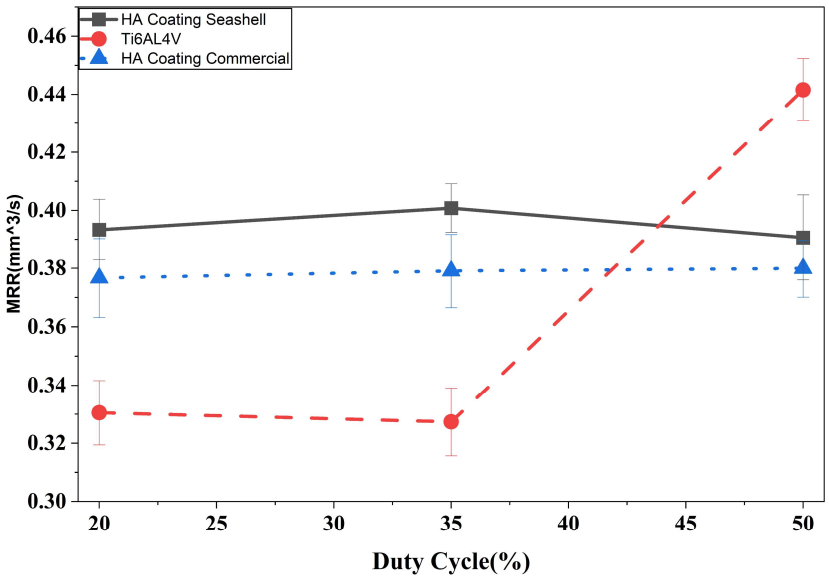


Figure 3.16 Variation of MRR with duty cycle for laser drilling

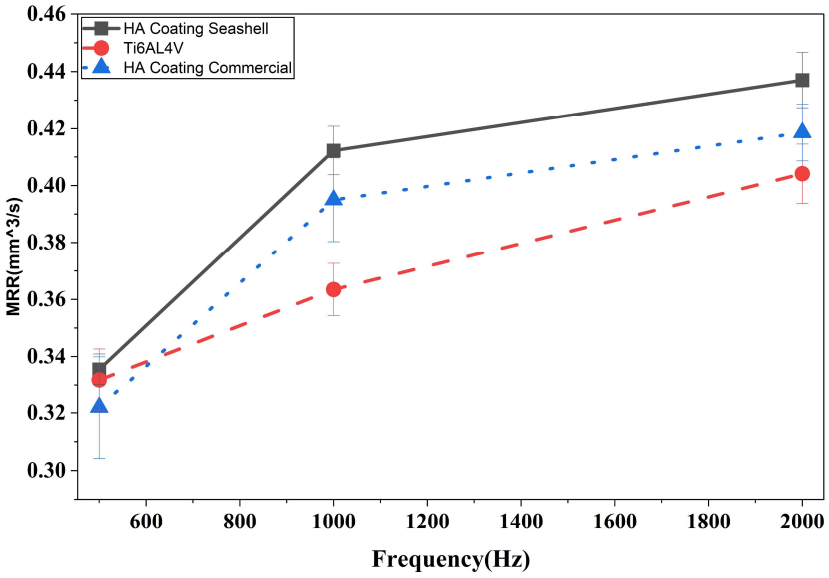


Figure 3.17 Variation of MRR with pulse frequency for laser drilling

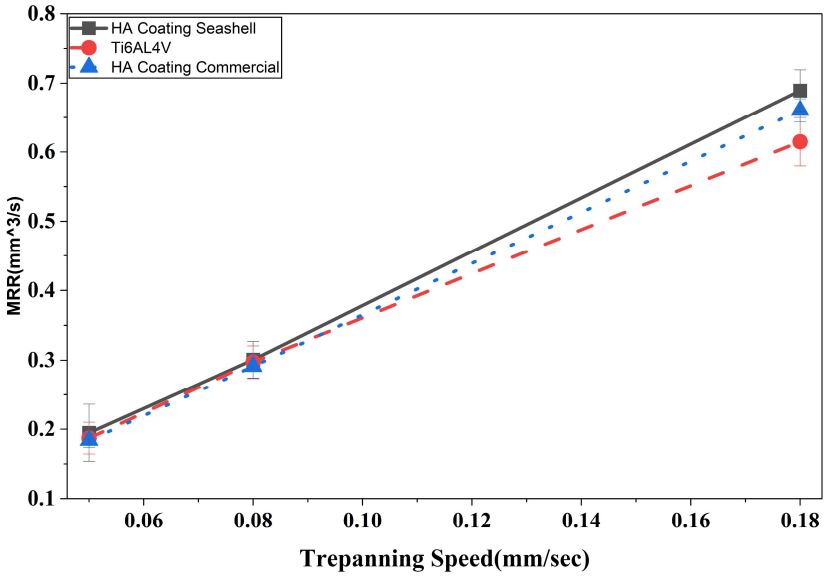


Figure 3.18 Variation of MRR with trepanning speed for laser drilling

3.8 Laser Drilling: Effect of Parameters on Taper Angle

The cylindricity of a hole is characterized by its taper angle. The main effect plots of laser drilling parameters on taper angle are presented in Figures 3.19, 3.20, and 3.21. Figure 3.19 shows the main effect of duty cycle on taper angle. All three samples exhibit increasing taper angles with duty cycle. The HA Coating Seashell shows the highest taper values across all duty cycle levels, followed by the HA Coating Commercial and uncoated Ti-6Al-4V. The consistently elevated taper in HA-coated samples compared to uncoated Ti-6Al-4V is due to coating delamination and thermal expansion mismatch at the coating-substrate interface, which promotes asymmetric material removal. The high amount of melted material removal from the top surface of the coating when the laser beam strikes causes the top diameter to be significantly larger than the bottom diameter. Figure 3.20 shows the main effect of pulse frequency on taper angle. All three samples exhibit a decreasing taper with increasing pulse frequency, attributed to more uniform energy distribution from higher pulse repetition rates resulting in more symmetric hole profiles. When the frequency is increased, molten material is allowed to re-solidify uniformly, reducing the taper deviation. Figure 3.21 shows the main effect of trepanning speed on taper angle. The taper angle remains essentially constant with trepanning speed for all samples, indicating that trepanning speed has negligible influence on

taper angle under the conditions tested. Higher taper angles are noticed in HA coated samples as compared to uncoated samples for all parameter conditions.

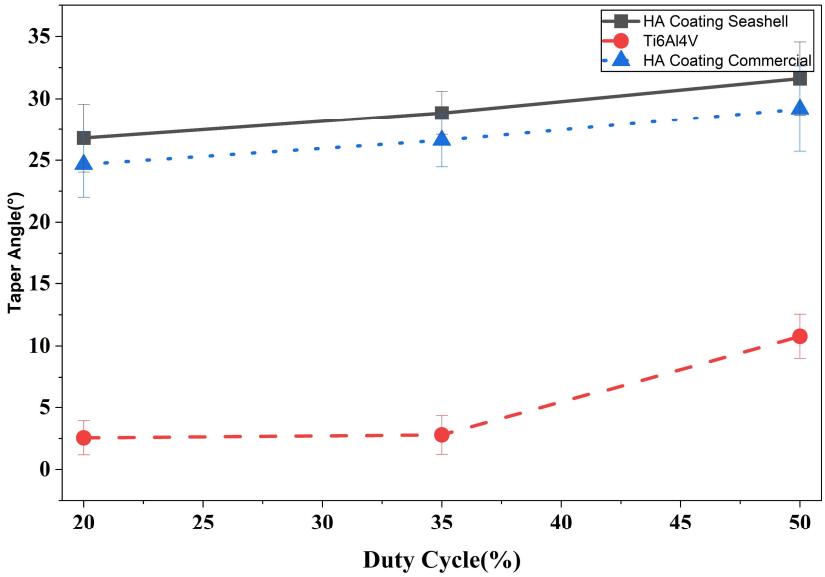


Figure 3.19 Variation of taper angle with duty cycle for laser drilling

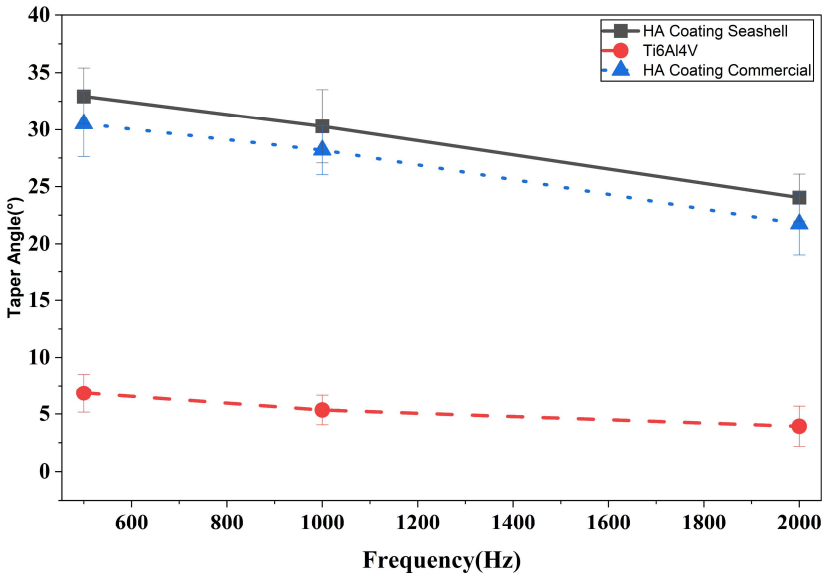


Figure 3.20 Variation of taper angle with pulse frequency for laser drilling

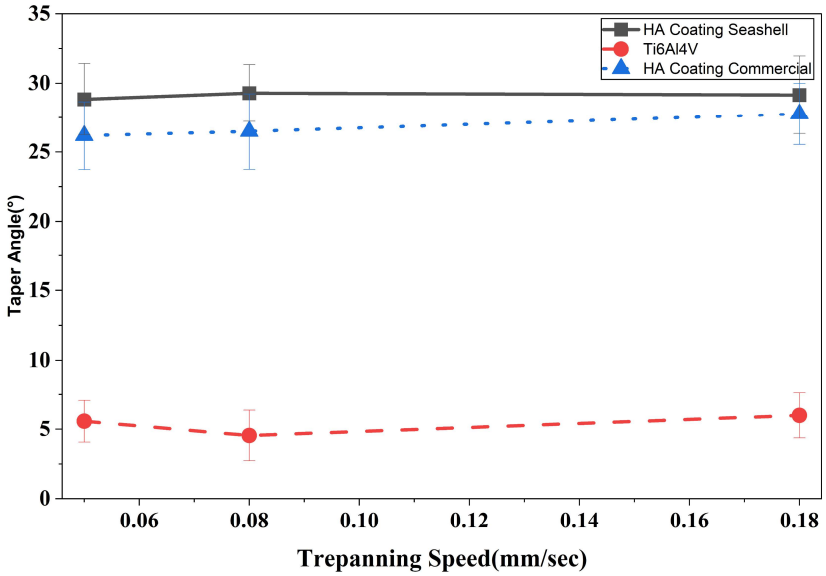
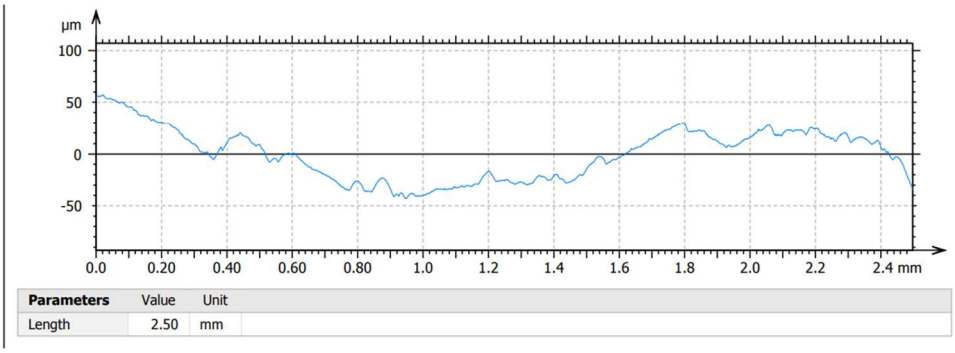


Figure 3.21 Variation of taper angle with trepanning speed for laser drilling

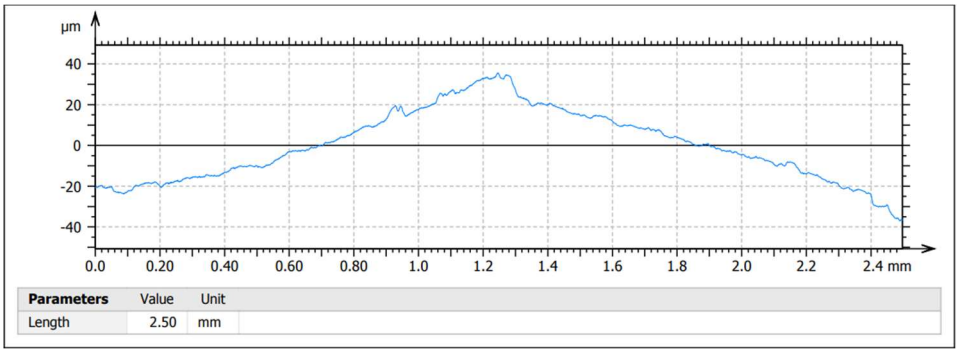
3.9 Surface Roughness of Drilled Holes

The inner surface roughness of drilled holes was measured using a stylus profilometer. Figure 3.22 presents the comparison of inner hole surface roughness for conventional and laser drilled Ti6Al4V holes. The average laser hole roughness was measured as 4.456 µm, while the average conventional hole roughness was 2.533 µm. The higher roughness in laser drilled holes is attributed to the thermal nature of the material removal process, which creates a recast layer with micro-cracks and resolidified material on the hole walls. Conventional drilling, being a mechanical process, produces smoother surfaces with more uniform tool marks.

The inner surface roughness profiles of conventionally and laser drilled Ti6Al4V holes were measured using a stylus profilometer with an evaluation length of 2.50 mm. Figure 3.22(a) shows the roughness profile for the conventionally drilled hole, exhibiting relatively uniform surface features. Figure 3.22(b) shows the roughness profile for the laser drilled hole, displaying more pronounced peaks and valleys due to the thermal nature of the laser removal process.



(a) Conventional drilling roughness profile



(b) Laser drilling roughness profile

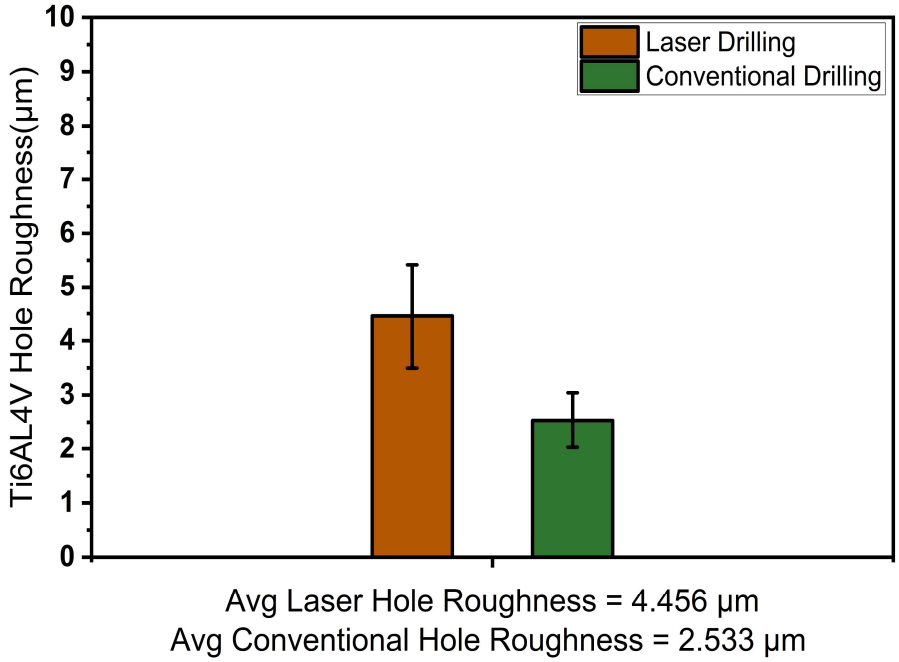


Figure 3.22 Comparison of inner hole surface roughness for conventional and laser drilled holes.

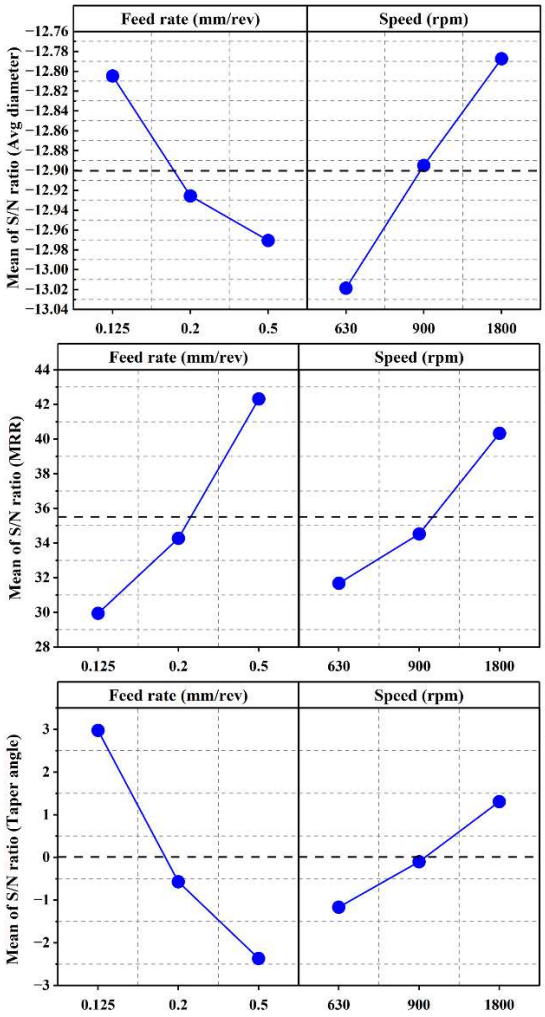
CHAPTER 4

OPTIMIZATION USING TAGUCHI S/N RATIO METHOD

A numerically larger S/N ratio indicates input parameters at which optimum responses are obtained. Taguchi uses the S/N ratio to measure the quality characteristic deviating from the desired value. In this study, the S/N ratio should have a maximum value to obtain optimum conditions. The results of responses are discussed in the following sections.

4.1 Main Effects: Conventional Drilling of Uncoated Samples

Table Main effect plots for S/N rations corresponding to the input parameters are represented in Figure 4.2 The S/N ratio is calculated by using the expression given in equation (4). Figure 4.1(a) describes the speed that has a larger difference in the vertical position of its plotted points and has a steeper slope. However, feed rate has a main effect on hole diameter, and it can be inferred that feed rate has minimal effect since it has a near-horizontal plot. On the other hand, feed rate has a main effect on MRR, but speed has minimal effect on the MRR, illustrated in Figure 4.1(b). Along with feed rates effect is dominated on the taper angle deviation of the hole, but speed has minimal effect on the taper angle, as shown in Figure 4.1(c). The measured drilling parameters and calculated S/N ratios for hole diameter, MRR, taper angle are shown in Table 4.1



Response table for S/N ratio (Hole diameter)		
Level	Feed rate	Speed
1	-12.8	-13.02
2	-12.93	-12.89
3	-12.97	-12.79
Delta	0.17	0.23
Rank	2	1

Response table for S/N ratio (MRR)		
Level	Feed rate	Speed
1	29.95	31.68
2	34.27	34.53
3	42.32	40.33
Delta	12.37	8.66
Rank	1	2

Response table for S/N ratio (Taper angle)		
Level	Feed rate	Speed
1	2.9736	-1.1667
2	-0.5693	-0.102
3	-2.3675	1.3055
Delta	5.3411	2.4722
Rank	1	2

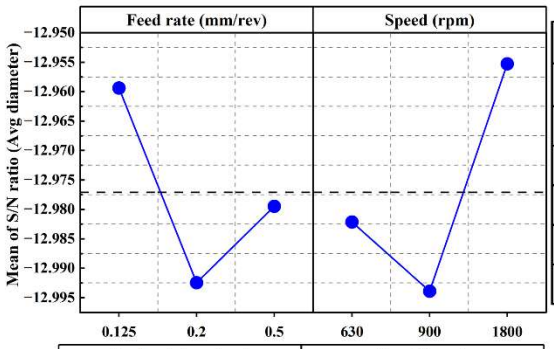
Figure 4.1 Main effect plot for (a) average diameter, (b) MRR, and (c) Taper angle of the holes in uncoated samples.

Table 4.1 Results of uncoated conventional drilling and their corresponding calculated S/N ratio

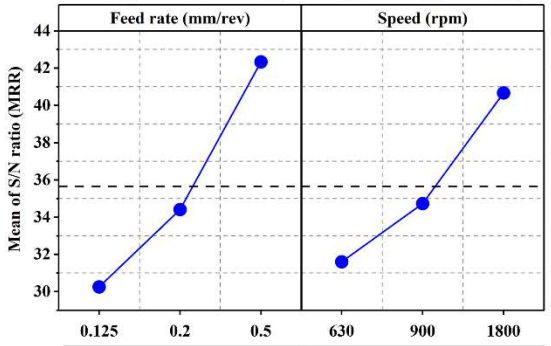
Exp. Run	Factors		Combination A:B	Measured parameters			Calculated S/N ratio		
	Feed (A)	Speed (B)		Hole dia.	MRR	Taper angle	Hole dia.	MRR	Taper angle
1	0.125	630	0.125:630	4.446	20.381	0.811	-12.960	26.184	1.812
2	0.125	900	0.125:900	4.383	28.297	0.704	-12.836	29.034	3.045
3	0.125	1800	0.125:1800	4.274	53.811	0.626	-12.617	34.617	4.062

4	0.2	630	0.200:630	4.486	33.192	1.222	-13.037	30.4206	-1.742
5	0.2	900	0.200:900	4.410	45.834	1.098	-12.889	33.2237	-0.812
6	0.2	1800	0.200:1800	4.390	90.838	0.907	-12.850	39.1654	0.846
7	0.5	630	0.500:630	4.497	83.386	1.508	-13.058	38.4219	-3.570
8	0.5	900	0.500:900	4.445	116.421	1.339	-12.958	41.3206	-2.538
9	0.5	1800	0.500:1800	4.412	229.419	1.121	-12.894	47.2126	-0.993

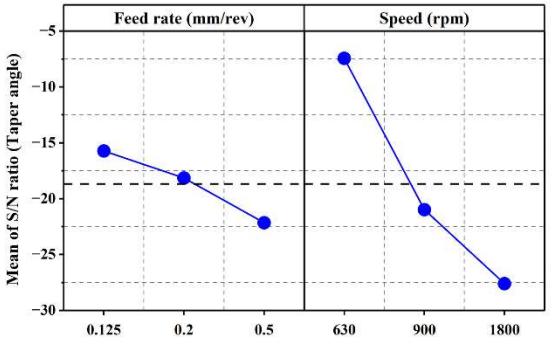
4.2 Main Effects: Conventional Drilling of HA Coating Seashell Samples



Response table for S/N ratio (Avg diameter)		
Level	Feed rate	Speed
1	-12.96	-12.98
2	-12.99	-12.99
3	-12.98	-12.96
Delta	0.03	0.04
Rank	2	1



Response table for S/N ratio (MRR)		
Level	Feed rate	Speed
1	30.25	31.6
2	34.4	34.72
3	42.34	40.67
Delta	12.08	9.06
Rank	1	2



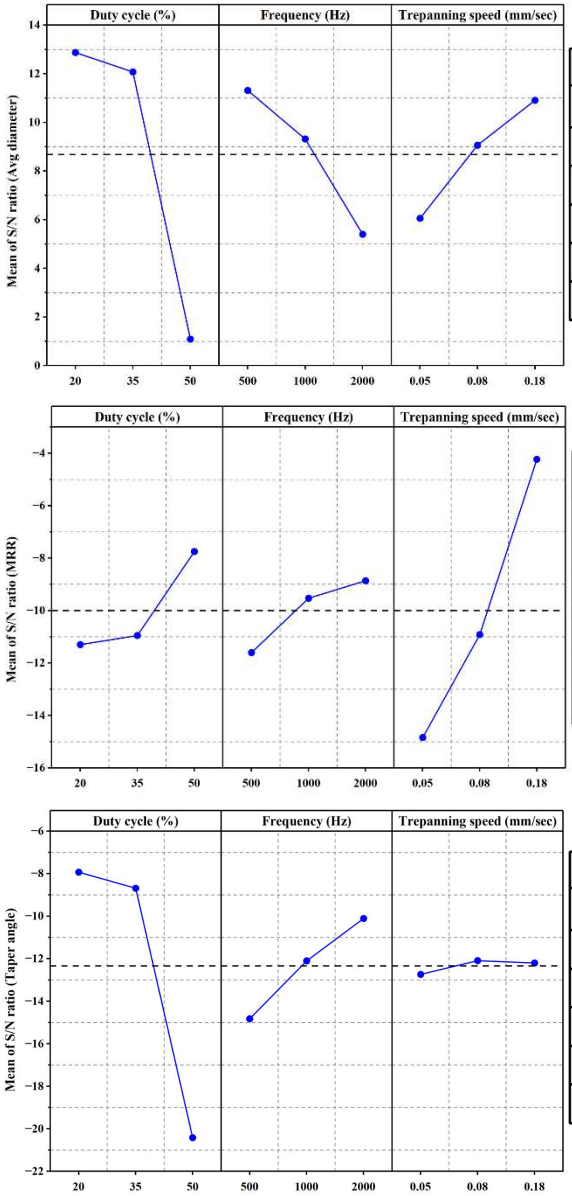
Response table for S/N ratio (Taper angle)		
Level	Feed rate	Speed
1	-15.729	-7.44
2	-18.152	-20.986
3	-22.153	-27.607
Delta	6.424	20.167
Rank	2	1

Figure 4.2 Main effect plot for (a) average diameter, (b) MRR, and (c) Taper angle of the holes in HA coated samples.

Table 4.2 Results of HA coated conventional drilling and their corresponding calculated S/N ratio

Exp. Run	Factors		Combination A:B	Measured parameters			Calculated S/N ratio		
	Feed (A)	Speed (B)		Hole dia.	MRR	Taper angle	Hole dia.	MRR	Taper angle
1	0.125	630	0.125:630	4.453	20.445	1.5275	-12.974	26.211	-3.6796
2	0.125	900	0.125:900	4.444	29.092	7.6942	-12.956	29.275	-17.7233
3	0.125	1800	0.125:1800	4.439	58.056	19.4632	-12.947	35.277	-25.7843
4	0.2	630	0.200:630	4.458	32.779	1.9092	-12.982	30.311	-5.617
5	0.2	900	0.200:900	4.489	47.48	11.4935	-13.043	33.530	-21.209
6	0.2	1800	0.200:1800	4.442	92.982	24.0687	-12.951	39.368	-27.6291
7	0.5	630	0.500:630	4.461	82.075	4.479	-12.989	38.284	-13.0236
8	0.5	900	0.500:900	4.457	117.04	15.896	-12.981	41.366	-24.0258
9	0.5	1800	0.500:1800	4.449	233.282	29.5421	-12.967	47.357	-29.4088

4.3 Main Effects: Laser Drilling of Uncoated Sample



Response table for S/N ratio (Avg diameter)			
Level	Duty cycle	Frequency	Speed
1	12.868	11.312	6.055
2	12.071	9.316	9.062
3	1.087	5.398	10.908
Delta	11.781	5.915	4.853
Rank	1	2	3

Response table for S/N ratio (MRR)			
Level	Duty cycle	Frequency	Speed
1	-11.298	-11.604	-14.846
2	-10.951	-9.531	-10.919
3	-7.749	-8.863	-4.233
Delta	3.549	2.741	10.613
Rank	2	3	1

Response table for S/N ratio (Taper angle)			
Level	Duty cycle	Frequency	Speed
1	-7.932	-14.828	-12.74
2	-8.688	-12.103	-12.093
3	-20.416	-10.106	-12.203
Delta	12.484	4.721	0.647
Rank	1	2	3

Figure 4.3 Main effect plot for (a) average diameter, (b) MRR, and (c) Taper angle of the holes in uncoated samples.

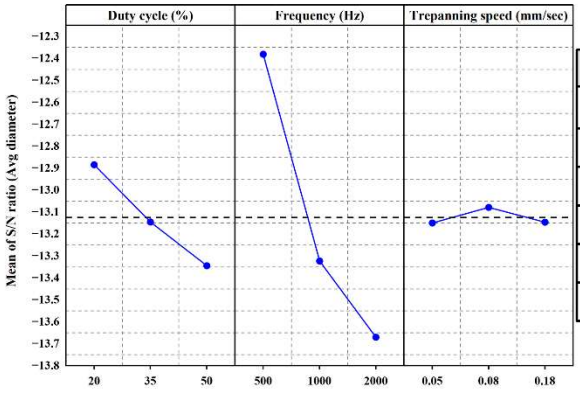
The main effect plotted using the laser drilling of uncoated samples and corresponding response table is illustrated in Figure 4.3 The main effect plot represents the influence of various parameters on the hole diameter is shown in Figure 4.3(a). It shows that effect of duty cycle is dominated rather than the frequency and trepanning speed on the hole diameter. Along with the response table indicates the rank which is in the first position. In addition, influence of trepanning speed on the MRR is noticed in the main effect plot shown in Figure

4.3(b). Furthermore, effect of duty cycle on the taper angle is observed in the main effect plot and corresponding response table is shown in Figure 4.3(c). The calculated S/N ratio value for duty cycle, frequency, and trepanning speed along measured parameters are presented in Table 4.3 For better dimensional accuracy of the hole and MRR, a combination of optimal duty cycle, and frequency with trepanning speed is required.

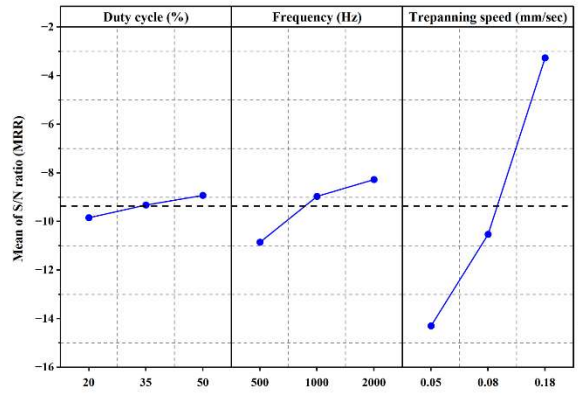
Table 4.3 Results of uncoated laser drilling and their corresponding calculated S/N ratio

Exp. Run	Factors			Combination A:B:C	Measured parameters			Calculated S/N ratio		
	DC (A)	Frq. (B)	Speed (C)		Hole dia.	MRR	Taper angle	Hole dia.	MRR	Taper angle
1	20	500	0.05	20:500:0.05	3.744	0.130	3.369	11.855	-17.660	-10.551
2	20	1000	0.08	20:1000:0.08	4.171	0.254	2.309	15.340	-11.883	-7.271
3	20	2000	0.18	20:2000:0.18	4.268	0.605	1.989	11.408	-4.351	-5.974
4	35	500	0.08	35:500:0.08	3.815	0.213	3.690	14.680	-13.430	-11.341
5	35	1000	0.18	35:1000:0.18	4.201	0.586	2.525	13.914	-4.627	-8.045
6	35	2000	0.05	35:2000:0.05	4.416	0.182	2.157	7.618	-14.795	-6.677
7	50	500	0.18	50:500:0.18	4.426	0.651	13.474	7.401	-3.721	-22.590
8	50	1000	0.05	50:1000 :0.05	5.162	0.248	11.208	-1.307	-12.082	-20.991
9	50	2000	0.08	50:2000:0.08	5.385	0.424	7.644	-2.832	-7.443	-17.666

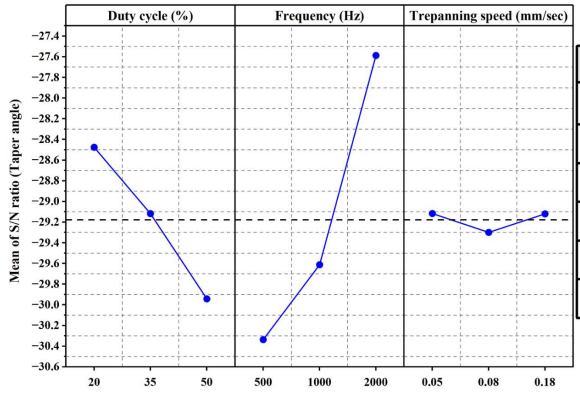
4.4 Main Effects: Laser Drilling of HA Coating Seashell Samples



Response table for S/N ratio (Avg diameter)			
Level	Duty cycle	Frequency	Speed
1	-12.88	-12.38	-13.15
2	-13.15	-13.32	-13.08
3	-13.34	-13.67	-13.15
Delta	0.46	1.29	0.07
Rank	2	1	3



Response table for S/N ratio (MRR)			
Level	Duty cycle	Frequency	Speed
1	-9.848	-10.855	-14.297
2	-9.327	-8.971	-10.535
3	-8.928	-8.277	-3.272
Delta	0.92	2.578	11.026
Rank	3	2	1



Response table for S/N ratio (Taper angle)			
Level	Duty cycle	Frequency	Speed
1	-28.48	-30.34	-29.12
2	-29.12	-29.61	-29.3
3	-29.94	-27.59	-29.12
Delta	1.47	2.75	0.18
Rank	2	1	3

Figure 4.4 Main effect plot for (a) average diameter, (b) MRR, and (c) Taper angle of the holes in HA coated samples.

Figure 4.4 describes the main effect plot of laser drilling of HA coated samples. The influence of various parameters on the hole diameter and their corresponding response table is shown in Figure 4.4(a). Observed that, frequency has higher effect on the hole diameter. However, trepanning speed shows negligible effect on the hole diameter. The effect of trepanning speed on the MRR shows higher shown in Figure 4.4(b). In addition, effect of

frequency is dominated on the taper angle rather than other parameters, as shown in Figure 4.4(c). Further, the calculated S/N ratios and measured parameters along with factors are included in Table 4.4

Table 4.4 Results of HA coated laser drilling and their corresponding calculated S/N ratio

Exp. Run		Factors		Combination A:B:C	Measured parameters			Calculated S/N ratio		
	DC (A)	Frq. (B)	Speed (C)		Hole dia.	MRR	Taper angle	Hole dia.	MRR	Taper angle
1	20	500	0.05	20:500:0.05	4.096	0.156	30.466	-12.247	-16.101	-29.676
2	20	1000	0.08	20:1000:0.08	4.452	0.290	28.146	-12.972	-10.748	-28.988
3	20	2000	0.18	20:2000:0.18	4.696	0.733	21.784	-13.434	-2.694	-26.762
4	35	500	0.08	35:500:0.08	4.139	0.250	32.862	-12.339	-12.014	-30.334
5	35	1000	0.18	35:1000:0.18	4.702	0.735	30.185	-13.446	-2.670	-29.595
6	35	2000	0.05	35:2000:0.05	4.814	0.216	23.509	-13.650	-13.296	-27.424
7	50	500	0.18	50:500:0.18	4.244	0.599	35.486	-12.557	-4.449	-31.001
8	50	1000	0.05	50:1000 :0.05	4.759	0.211	32.551	-13.551	-13.494	-30.251
9	50	2000	0.08	50:2000:0.08	4.969	0.361	26.843	-13.925	-8.841	-28.576

Table 4.5 Optimal combination of parameters obtained by S/N ratios analysis.

Drilling type	**Material**	**Response**	**S/N ratio**	**Best parameters**
Conventional	Uncoated	Avg diameter	-12.8503	Feed = 0.2 mm/rev
				Speed = 1800 rpm
Conventional	Uncoated	MRR	39.0861	Feed = 0.2 mm/rev
				Speed = 1800 rpm
Conventional	Uncoated	Taper angle	1.8127	Feed = 0.125 mm/rev
				Speed = 630 rpm
Conventional	HA coated	Avg diameter	-12.9516	Feed = 0.2 mm/rev
				Speed = 1800 rpm
Conventional	HA coated	MRR	39.3680	Feed = 0.2 mm/rev
				Speed = 1800 rpm
Conventional	HA coated	Taper angle	-3.6797	Feed = 0.125 mm/rev
				Speed = 630 rpm
Laser	Uncoated	Avg diameter	15.3401	DC = 20 %
				Frequency = 1000 Hz
				Trepanning speed = 0.08 mm/s
Laser	Uncoated	MRR	- 4.6276	DC = 35 %
				Frequency = 1000 Hz
				Trepanning speed = 0.18 mm/s
Laser	Uncoated	Taper angle	-5.5935	DC = 35 %
				Frequency = 1000 Hz
				Trepanning speed = 0.18 mm/s
Laser	HA coated	Avg diameter	-12.3390	DC = 35 %
				Frequency = 500 Hz
				Trepanning speed = 0.08 mm/s
Laser	HA coated	MRR	-4.1867	DC = 35 %
				Frequency = 1000 Hz
				Trepanning speed = 0.18 mm/s
Laser	HA coated	Taper angle	-9.1346	DC = 35 %
				Frequency = 2000 Hz
				Trepanning speed = 0.08 mm/s

CHAPTER 5

MULTI-RESPONSE OPTIMIZATION: GRA AND ANOVA

5.1 Conventional Drilling of Uncoated Samples

In this section, Taguchi GRA is employed to optimize the multi-response factor of the uncoated Ti-6Al-4V drilled by the conventional process. Response normalization is mainly divided into three categories based on the expected nature of the response values. In the present study, the MRR increases with both feed rate and spindle speed. However, the hole diameter and taper angle increase with feed rate, which is undesirable. Hence, hole diameter and taper angle are considered as smaller-the-better, and MRR is considered as larger-the-better.

Table 5.1 Reference and deviation sequences after data pre-processing for uncoated conventional drilling.

Exp. Run	Reference Sequences, Xi*	Reference Sequences, Xi*	Reference Sequences, Xi*	Deviation Sequences, 0i	Deviation Sequences, 0i	Deviation Sequences, 0i
Exp. Run	Hole dia.	MRR	Taper angle	Hole dia.	MRR	Taper angle
1	0.2269	0.0000	0.7900	0.7731	1.0000	0.2100
2	0.5099	0.0379	0.9117	0.4901	0.9621	0.0883
3	1.0000	0.1599	1.0000	0.0000	0.8401	0.0000
4	0.0494	0.0613	0.3246	0.9506	0.9387	0.6754
5	0.3886	0.1218	0.4653	0.6114	0.8782	0.5347
6	0.4784	0.3371	0.6817	0.5216	0.6629	0.3183
7	0.0000	0.3014	0.0000	1.0000	0.6986	1.0000
8	0.2305	0.4594	0.1915	0.7695	0.5406	0.8085
9	0.3778	1.0000	0.4391	0.6222	0.0000	0.5609

Table 5.2 GRC and WGRG with S/N ratios (uncoated, conventional).

Exp. Run	**GRC Coefficient (= 0.5)**	**GRC Coefficient (= 0.5)**	**GRC Coefficient (= 0.5)**	**WGRG**	**S/N Ratio of GRG**	**Rank**
Exp. Run	Hole dia.	MRR	Taper angle	WGRG	S/N Ratio of GRG	Rank
1	0.3927	0.7042	0.3333	0.4930	-6.1438	5
2	0.5050	0.8499	0.3420	0.5966	-4.4869	2
3	1.0000	1.0000	0.3731	0.8746	-1.1636	1

4	0.3447	0.4254	0.3475	0.3743	-8.5353	8
5	0.4499	0.4832	0.3628	0.4445	-7.0432	6
6	0.4894	0.6111	0.4299	0.5213	-5.6580	4
7	0.3333	0.3333	0.4172	0.3501	-9.1167	9
8	0.3938	0.3821	0.4805	0.4069	-7.8096	7
9	0.4456	0.4713	1.0000	0.5657	-4.9478	3

Table 5.3 Response table of WGRGs (uncoated, conventional).

Factors	**Level 1**	**Level 2**	**Level 3**	**Delta**	**Rnak**
Feed (mm/rev)	0.6547 *	0.4467	0.4409	0.2138	2
Speed (RPM)	0.4058	0.4827	0.6539 *	0.2481	1

ANOVA confirms that feed rate and speed are the dominant parameters, contributing 43.91% and 47.74% respectively to the overall performance. Both factors are statistically significant: feed rate ($P = 0.0255$) and spindle speed ($P = 0.0221$), both with $P < 0.05$. The error contribution was 8.34%. The weights assigned for this multi-response optimization were: Average Hole Diameter (D_avg) = 0.44, Taper Angle = 0.36, and Material Removal Rate (MRR) = 0.20, reflecting the priority of dimensional accuracy and geometric precision over productivity. The optimal combination A1B3 (Feed = 0.125 mm/rev, Speed = 1800 RPM) achieved a WGRG of 0.8746, representing a 68.80% improvement over the mean performance (0.5181).

Table 5.4 ANOVA for WGRG (uncoated, conventional).

Source	**DF**	**Seq SS**	**Adj MS**	**F-Value**	**P-Value**	**Contribution**
Feed	2	0.089016	0.044508	10.5244	0.0255 *	43.91 %
Speed	2	0.096786	0.048393	11.4431	0.0221 *	47.74 %
Error	4	0.016916	0.004229	-	-	8.34 %
Total	8	0.202717	-	-	-	100.00 %

5.2 Conventional Drilling of HA Coating Seashell Samples

Table 5.5 GRC and WGRG with S/N ratios (HA Coating Seashell, conventional).

Exp.	**GRC Dia.**	**GRC MRR**	**GRC Taper**	**WGRG**	**S/N Ratio**	**Rank**
1	0.6423	0.3333	0.4385	0.4990	-6.0383	6
1	0.6423	0.4385	0.3333	0.5071	-5.8976	6

2	0.8339	0.6943	0.3426	0.6854	-3.2813	4
3	1.0000	1.0000	0.3778	0.8756	-1.1543	1
4	0.5748	0.3833	0.3467	0.4602	-6.7403	7
5	0.3333	0.5843	0.3642	0.4298	-7.3339	9
6	0.9179	0.9735	0.4313	0.8406	-1.5083	2
7	0.5313	0.3333	0.4131	0.4364	-7.2027	8
8	0.5816	0.4936	0.4779	0.5292	-5.5279	5

Table 5.6 Response table of WGRGs (HA Coating Seashell, conventional).

Factors	**Level 1**	**Level 2**	**Level 3**	**Delta**	**Rank**
Feed (mm/rev)	0.6894 *	0.5769	0.5916	0.1125	2
Speed (RPM)	0.4679	0.5481	0.8418 *	0.3739	1

ANOVA confirms that spindle speed is the dominant factor, contributing 85.96% to the overall performance, while feed rate contributes only 8.29%. The speed factor is highly statistically significant (P = 0.0039, P < 0.01), while feed rate is not statistically significant (P = 0.1679). The error contribution was 5.75%. The same weight distribution of 0.44, 0.36, and 0.20 for D_avg, Taper Angle, and MRR respectively was applied. The optimal combination A1B3 (Feed = 0.125 mm/rev, Speed = 1800 RPM) achieved a WGRG of 0.8756, representing a 41.79% improvement over the mean performance (0.6175).

Table 5.7 ANOVA for WGRG (HA Coating Seashell, conventional).

Source	**DF**	**Seq SS**	**Adj MS**	**F-Value**	**P-Value**	**Contribution**
Feed	2	0.022420	0.011210	2.8816	0.1679	8.29 %
Speed	2	0.232477	0.116238	29.8798	0.0039 *	85.96 %
Error	4	0.015561	0.003890	-	-	5.75 %
Total	8	0.270457	-	-	-	100.00 %

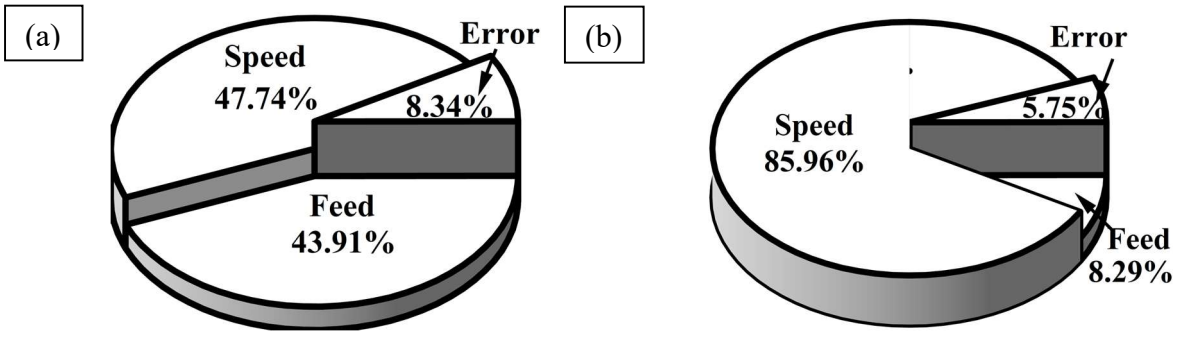


Figure 5.1 ANOVA contribution: (a) uncoated and (b) HA Coating Seashell — conventional drilling.

5.3 Laser Drilling of Uncoated Samples

Table 5.8 GRC and WGRG with S/N ratios (uncoated, laser).

Exp. Run	**GRC Co-efficient (= 0.5)**	**GRC Co-efficient (= 0.5)**	**GRC Co-efficient (= 0.5)**	**WGRG**	**S/N Ratio of GRG**	**Rank**
Exp. Run	Hole dia.	MRR	Taper angle	WGRG	S/N Ratio of GRG	Rank
1	0.7306	0.8062	0.3333	0.6784	-3.3708	6
2	0.8020	0.9472	0.3961	0.7731	-2.2354	3
3	0.7204	1.0000	0.8510	0.8472	-1.4405	1
4	0.7897	0.7715	0.3725	0.6997	-3.1017	4
5	0.7747	0.9147	0.8013	0.8304	-1.6140	2
6	0.6248	0.9716	0.3567	0.6960	-3.1475	5
7	0.6190	0.3333	1.0000	0.5923	-4.5485	7
8	0.3734	0.3838	0.3926	0.3810	-8.3819	9
9	0.3333	0.5038	0.5341	0.4348	-7.2334	8

Table 5.9 Response table of WGRGs (uncoated, laser).

Factors	**Level 1**	**Level 2**	**Level 3**	**Delta**	**Rnak**
DC (%)	0.7662 *	0.7421	0.4694	0.2968	1
Freq (Hz)	0.6568	0.6615 *	0.6593	0.0047	3
Tre Speed (mm/s)	0.5851	0.6359	0.7566 *	0.1715	2

ANOVA confirms that duty cycle is the overwhelmingly dominant factor, contributing 76.47% to the overall performance, while trepanning speed contributes 21.85% and frequency has negligible influence (0.02%). The duty cycle is statistically significant ($P = 0.0213$, $P < 0.05$). The error contribution was minimal (1.67%), indicating excellent experimental design. The same weight distribution (D_avg: 0.44, Taper Angle: 0.36, MRR: 0.20) was applied. The optimal combination A1B2C3 (DC = 20%, Freq = 1000 Hz, Speed = 0.18 mm/s) achieved a WGRG of 0.8506, representing a 28.64% improvement over the mean performance (0.6610).

Table 5.10 ANOVA for WGRG (uncoated, laser).

Source	**DF**	**Seq SS**	**Adj MS**	**F-Value**	**P-Value**	**Contribution**

DC (%)	2	0.163028	0.081514	45.8717	0.0213 *	76.47 %
Freq (Hz)	2	0.000033	0.000017	0.0093	0.9908	0.02 %
Tre Speed	2	0.046582	0.023291	13.1069	0.0709	21.85 %
Error	2	0.003554	0.001777	-	-	1.67 %
Total	8	0.213198	-	-	-	100.00 %

5.4 Laser Drilling of HA Coating Seashell Samples

Table 5.11 GRC and WGRG with S/N ratios (HA Coating Seashell, laser).

Exp. Run	**GRC Co-efficient (= 0.5)**	**GRC Co-efficient (= 0.5)**	**GRC Co-efficient (= 0.5)**	**WGRG**	**S/N Ratio of GRG**	**Rank**
Exp. Run	Hole dia.	MRR	Taper angle	WGRG	S/N Ratio of GRG	Rank
1	0.8344	0.4411	0.3333	0.5926	-4.5449	2
2	0.5171	0.5185	0.3939	0.4930	-6.1437	7
3	0.4105	1.0000	0.9930	0.7392	-2.6245	1
4	0.7765	0.3821	0.3739	0.5540	-5.1299	3
5	0.4082	0.4492	1.0000	0.5413	-5.3309	5
6	0.3732	0.7989	0.3580	0.5234	-5.6231	6
7	0.6644	0.3333	0.6800	0.5483	-5.2193	4
8	0.3895	0.3889	0.3558	0.3825	-8.3464	9
9	0.3333	0.5752	0.4362	0.4410	-7.1119	8

Table 5.12 Response table of WGRGs (HA Coating Seashell, laser).

Factors	**Level 1**	**Level 2**	**Level 3**	**Delta**	**Rnak**
DC (%)	0.6083 *	0.5396	0.4573	0.1510	1
Freq (Hz)	0.5650	0.4723	0.5679 *	0.0956	3
Tre Speed (mm/s)	0.4995	0.4960	0.6096 *	0.1136	2

ANOVA suggests that duty cycle is the dominant parameter, contributing 43.08% to the overall performance. Trepanning speed contributes 31.48% and frequency contributes 22.29%. Under the weighted framework with only 2 error degrees of freedom, no factor achieves statistical significance at the 5% level (DC: P = 0.0683, Freq: P = 0.1241, Speed: P = 0.0912). The ranking and contribution percentages serve as the primary optimization metrics. The error contribution was minimal (3.16%), suggesting that the experimental design successfully captured the majority of the process variability. The same weight distribution (D_avg: 0.44, Taper Angle: 0.36, MRR: 0.20) was applied.

Table 5.13 ANOVA for WGRG (HA Coating Seashell, laser).

Source	DF	Seq SS	Adj MS	F-Value	P-Value	Contribution
DC (%)	2	0.034286	0.017143	13.6443	0.0683	43.08 %
Freq (Hz)	2	0.017738	0.008869	7.0590	0.1241	22.29 %
Tre Speed	2	0.025051	0.012526	9.9694	0.0912	31.48 %
Error	2	0.002513	0.001256	-	-	3.16 %
Total	8	0.079588	-	-	-	100.00 %

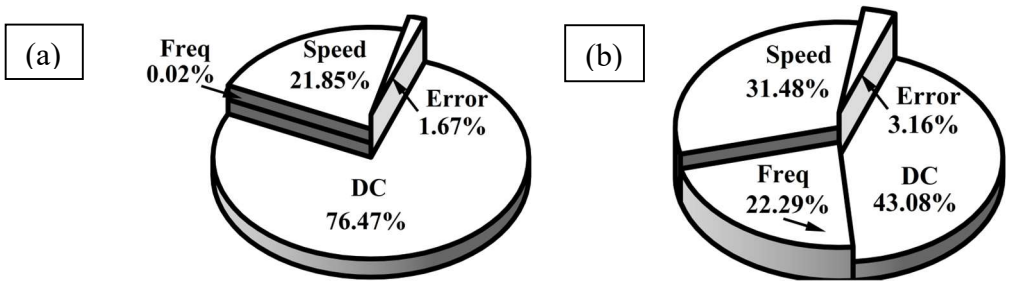


Figure 5.2 ANOVA contribution: (a) uncoated and (b) HA Coating Seashell — laser drilling.

5.5 Conventional Drilling of HA Coating Commercial Samples

Taguchi GRA is employed to optimize the multi-response factor of the HA Coating Commercial sample drilled by the conventional process. Consistent weights were assigned to the performance responses across all three materials: 0.44 to Average Hole Diameter (D_avg), 0.36 to Taper Angle, and 0.20 to Material Removal Rate (MRR). Table 5.14 presents the Calculated GRC, WGRG, and S/N ratios. Experimental Run 3 exhibited the highest WGRG of 0.6249, indicating it is the closest to the ideal multi-objective solution under the weighted evaluation framework.

Table 5.14 GRC and WGRG with S/N ratios (HA Coating Commercial, conventional).

Exp.	GRC Dia.	GRC MRR	GRC Taper	WGRG	S/N Ratio	Rank
1	0.3957	0.4388	0.3333	0.3987	-7.9863	7
2	0.4215	0.5295	0.3424	0.4446	-7.0414	4
3	0.4305	1.0000	0.3774	0.6249	-4.0838	1
4	0.3583	0.3632	0.3479	0.3580	-8.9227	8
5	0.4089	0.4908	0.3632	0.4292	-7.3459	5
6	0.4231	0.4974	0.4312	0.4515	-6.9075	3
7	0.3333	0.3333	0.4206	0.3508	-9.0998	9
8	0.4000	0.4259	0.4797	0.4253	-7.4268	6
9	0.4190	0.4456	1.0000	0.5448	-5.2756	2

Table 5.15 Response table of WGRGs (HA Coating Commercial, conventional).

Factors	Level 1	Level 2	Level 3	Delta	Rank
Feed (mm/rev)	0.4894 *	0.4129	0.4403	0.0765	2
Speed (RPM)	0.3692	0.4330	0.5404 *	0.1712	1

Table 5.16 ANOVA for WGRG (HA Coating Commercial, conventional).

Source	DF	Seq SS	Adj MS	F-Value	P-Value	Contribution
Feed	2	0.009015	0.004508	2.3728	0.2092	14.65 %
Speed	2	0.044921	0.022461	11.8231	0.0209 *	73.00 %
Error	4	0.007599	0.001900	-	-	12.35 %
Total	8	0.061535	-	-	-	100.00 %

The Analysis of Variance (ANOVA) performed on the WGRG values (Table 5.16) confirms that Spindle Speed is the dominant factor, contributing 73.00% to the overall weighted performance, while Feed Rate contributes only 14.65%. The Speed factor was found to be statistically significant ($P = 0.0209$, $P < 0.05$). The error contribution was 12.35%. The optimal combination of parameters for HA Coating Commercial conventional drilling is found to be A1B3 (Feed = 0.125 mm/rev, Speed = 1800 RPM).

5.6 Laser Drilling of HA Coating Commercial Samples

Taguchi WGRA is employed to optimize the multi-response parameter characteristics of the HA Coating Commercial sample drilled by the laser process. The same weight distribution of 0.44 for Average Hole Diameter (D_avg), 0.36 for Taper Angle, and 0.20 for Material Removal Rate (MRR) was applied consistently. Table 5.17 illustrates the computed GRC values and the WGRG. Run 3 (DC = 20%, Freq = 2000 Hz, Tre Speed = 0.18 mm/s) achieved the highest WGRG of 0.7437 under the weighted evaluation.

Table 5.17 GRC and WGRG with S/N ratios (HA Coating Commercial, laser).

Exp.	GRC Dia.	GRC MRR	GRC Taper	WGRG	S/N Ratio	Rank
1	0.8393	0.4809	0.3333	0.6091	-4.3066	3
2	0.5981	0.5738	0.3997	0.5497	-5.1979	7
3	0.4345	0.9791	1.0000	0.7437	-2.5726	1
4	0.9150	0.4032	0.3775	0.6233	-4.1067	2
5	0.4848	0.4407	0.9652	0.5650	-4.9590	6
6	0.3718	1.0000	0.3583	0.5953	-4.5060	5
7	0.7792	0.3333	0.6963	0.6021	-4.4067	4
8	0.4085	0.4041	0.3613	0.3975	-8.0138	9
9	0.3333	0.6803	0.4419	0.4799	-6.3763	8

Table 5.18 Response table of WGRGs (HA Coating Commercial, laser).

Factors	Level 1	Level 2	Level 3	Delta	Rank
DC (%)	0.6341 *	0.5945	0.4932	0.1410	1
Freq (Hz)	0.6115 *	0.5041	0.6063	0.1074	2
Tre Speed (mm/s)	0.5339	0.5510	0.6369 *	0.1030	3

Table 5.19 ANOVA for WGRG (HA Coating Commercial, laser).

Source	DF	Seq SS	Adj MS	F-Value	P-Value	Contribution
DC (%)	2	0.031710	0.015855	13.5058	0.0689	42.64 %
Freq (Hz)	2	0.022018	0.011009	9.3780	0.0964	29.61 %
Tre Speed	2	0.018285	0.009143	7.7880	0.1138	24.59 %
Error	2	0.002348	0.001174	-	-	3.16 %
Total	8	0.074361	-	-	-	100.00 %

The Analysis of Variance (ANOVA) performed on the WGRG values (Table 5.19) confirms that DC (%) is the dominant factor, contributing 42.64% to the overall weighted performance, while Frequency contributes 29.61% and Traverse Speed contributes 24.59%. The error contribution was minimal (3.16%), validating the experimental design. The optimal combination of parameters for HA Coating Commercial laser drilling is A1B1C3 (DC = 20%, Freq = 500 Hz, Speed = 0.18 mm/s).

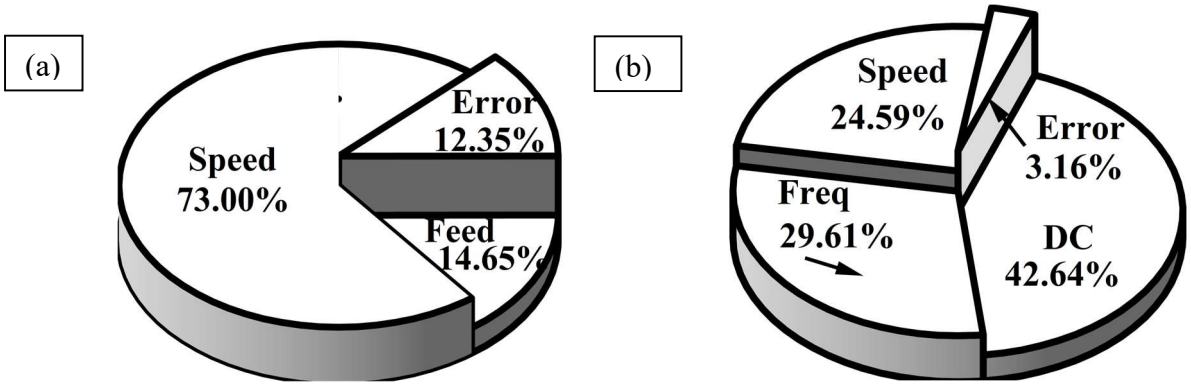


Figure 5.3 ANOVA contribution of HA Coating Commercial: (a) Conventional and (b) laser drilling.

5.7 Optimal Drilling Parameters Summary

Table 5.20 Optimal drilling parameters after Taguchi WGRG multi-objective optimization.

Drilling Type	Material	Parameter (A)	Parameter (B)	Parameter (C)	Optimal	Best WGRG
Conventional	Uncoated (Ti-6Al-4V)	Feed=0.125 mm/rev	Speed=1800 rpm	—	A1B3	0.8746
Conventional	HA Coating Seashell	Feed=0.125 mm/rev	Speed=1800 rpm	—	A1B3	0.8756
Conventional	HA Coating Commercial	Feed=0.125 mm/rev	Speed=1800 rpm	—	A1B3	0.6249
Laser	Uncoated (Ti-6Al-4V)	DC=20%	Freq=1000 Hz	Speed=0.18 mm/s	A1B2C3	0.8506
Laser	HA Coating Seashell	DC=20%	Freq=2000 Hz	Speed=0.18 mm/s	A1B3C3	0.7392
Laser	HA Coating Commercial	DC=20%	Freq=500 Hz	Speed=0.18 mm/s	A1B1C3	0.7437

CHAPTER 6

CONCLUSIONS AND FUTURE SCOPE

6.1 Conclusions

The present study investigated the machinability of biogenic hydroxyapatite (HA) coatings (seashell-derived) and commercial HA coatings deposited on Ti-6Al-4V substrates by flame spraying. Three sample types—bare Ti-6Al-4V alloy, HA Coating Seashell, and HA Coating Commercial—were machined by conventional drilling and laser trepanning. All experiments were conducted using Taguchi L9 orthogonal arrays with varying parameters. The main effect plots and multi-response optimization using Weighted Grey Relational Analysis (WGRA) with ANOVA yielded the following key conclusions:

- Seashell-derived HA coatings were successfully deposited on grit-blasted Ti-6Al-4V substrates by the flame spraying technique at standoff distances of 70, 90, and 110 mm. The coating thickness ranged from 236.79 to 369.28 μm and surface roughness from 12.85 to 15.375 μm.
- In conventional drilling, the main effect analysis showed that both feed rate and spindle speed significantly influence hole quality. The main effect plots confirmed that spindle speed is the dominant factor for hole diameter and taper angle (holes closer to nominal at higher speeds), while feed rate dominates MRR. For all three sample types, MRR increases linearly with both feed rate and spindle speed.
- HA Coating Seashell substrates exhibited larger hole diameters and significantly higher taper angles compared to uncoated Ti-6Al-4V in conventional drilling, attributed to the brittle fracture and delamination behaviour of the ceramic coating. The HA Coating Commercial showed intermediate behaviour between the uncoated and seashell-coated samples. At higher spindle speeds, taper angle reduced dramatically for both HA-coated sample types.
- In laser trepanning, the main effect analysis revealed that duty cycle was the most influential parameter affecting hole diameter and taper angle for all sample types. Higher duty cycle increased both diameter deviation and taper angle. Pulse frequency showed increasing diameter and decreasing taper trends, while trepanning speed was the dominant factor for MRR, showing a strong linear relationship across all three samples.

- HA Coating Seashell samples exhibited significantly higher taper angles than uncoated Ti-6Al-4V in laser drilling, linked to thermal expansion mismatch, lower adhesion strength, and micro-cracking at the coating-substrate interface. The HA Coating Commercial showed similar behaviour with taper values between the seashell-coated and uncoated samples.
- MRR values were comparable between coated and uncoated samples for both drilling processes, with differences under 5% in conventional drilling.
- Multi-response optimization using Taguchi-based Weighted Grey Relational Analysis (WGRG) with a uniform weight distribution of 0.44 for Average Hole Diameter (D_avg), 0.36 for Taper Angle, and 0.20 for MRR identified the following optimal parameters:
  - Conventional drilling (uncoated): Feed = 0.125 mm/rev, Speed = 1800 rpm (A1B3), WGRG = 0.8746 (68.80% improvement over mean)
  - Conventional drilling (HA Coating Seashell): Feed = 0.125 mm/rev, Speed = 1800 rpm (A1B3), WGRG = 0.8756 (41.79% improvement over mean)
  - Laser drilling (uncoated): DC = 20%, Freq = 1000 Hz, Speed = 0.18 mm/s (A1B2C3), WGRG = 0.8506 (28.64% improvement over mean)
  - Laser drilling (HA Coating Seashell): DC = 20%, Freq = 2000 Hz, Speed = 0.18 mm/s (A1B3C3), WGRG = 0.7392 (38.00% improvement over mean)
  - Conventional drilling (HA Coating Commercial): Feed = 0.125 mm/rev, Speed = 1800 rpm (A1B3), WGRG = 0.6249
  - Laser drilling (HA Coating Commercial): DC = 20%, Freq = 500 Hz, Speed = 0.18 mm/s (A1B1C3), WGRG = 0.7437
- ANOVA confirmed that for HA Coating Seashell conventional drilling, spindle speed contributed 85.96% to the WGRG and was highly statistically significant (P = 0.0039). Feed rate contributed only 8.29% with error of 5.75%. For uncoated conventional drilling, feed rate and speed contributed 43.91% and 47.74% respectively, both statistically significant (P = 0.0255 and P = 0.0221).

For HA Coating Commercial conventional drilling, ANOVA showed speed contributing 73.00% to the WGRG (P = 0.0209), making it the dominant factor, while feed rate contributed 14.65%. For HA Coating Commercial laser drilling, duty cycle emerged as the dominant factor (42.64%), followed by frequency (29.61%) and traverse speed (24.59%), with minimal error contribution (3.16%).

- For laser drilling, duty cycle contributed 76.47% to the WGRG of uncoated samples (P = 0.0213, statistically significant), with trepanning speed contributing 21.85% and frequency having negligible effect (0.02%). The error contribution was only 1.67%. For HA Coating Seashell laser drilling, duty cycle (43.08%), trepanning speed (31.48%), and frequency (22.29%) shared influence more evenly, with no factor achieving statistical significance at $P < 0.05$ due to limited error degrees of freedom (DF = 2).
- Under low feed rate and high speed, the HA coatings showed satisfactory machinability in conventional drilling with reduced taper angles and improved dimensional accuracy. The machinability of HA-coated samples by laser trepanning was improved at lower duty cycle and higher frequency, which produced more symmetric hole profiles with reduced taper deviation.

6.2 Future Scope

1. Detailed microstructural analysis (SEM, EDS) of the drilled hole surfaces and cross-sections for both conventional and laser drilled samples.
2. Investigation of tool wear mechanisms during conventional drilling of HA Coating Seashell samples.
3. Optimization using advanced methods such as RSM, ANN, or genetic algorithms for broader parameter ranges.
4. Study of the effect of different coating thicknesses and standoff distances on machinability.
5. Biocompatibility testing of the machined surfaces to evaluate the suitability for clinical implant applications.
6. Extension to other machining processes such as micro-milling and ultrasonic machining of HA Coating Seashell implants.

REFERENCES

[1] C.H. Tsai, H.W. Chen, "Laser shaping of ceramic by fracture machining technique," J. Mater. Process. Technol., vol. 136, pp. 158–165, 2003.

[2] S. Sharif, E.A. Rahim, "Performance evaluation of coated and uncoated carbide drills when drilling Ti-6Al-4V," J. Mater. Process. Technol., vol. 185, pp. 72–78, 2007.

[3] M. Avvari, M. Manjaiah et al., "Optimization of hole characteristics during pulse Nd:YAG laser drilling of commercially pure titanium alloy," Lasers Manuf. Mater. Process., vol. 4, pp. 76–91, 2017.

[4] S. Chatterjee, S.S. Mahapatra et al., "An experimental study on drilling of titanium alloy using CO_2 laser," Sādhanā, vol. 43, no. 8, pp. 131, 2018.

[5] C.G. Yuan, A. Pramanik et al., "Drilling of titanium alloy (Ti6Al4V)—a review," Machining Science and Technology, vol. 25, no. 4, pp. 637–702, 2021.

[6] B. Vasudevan, Y. Natarajan et al., "Insights into drilling film cooling holes on ceramic-coated nickel-based superalloys," Archives of Civil and Mechanical Engineering, vol. 22, no. 1, pp. 25, 2022.

[7] Various, "Water-jet guided laser drilling of thermal barrier coatings on nickel-based superalloys," ScienceDirect, 2022.

[8] B. Zhang et al., "Grinding of nanostructured Al_2O_3-TiO_2 and WC-Co coatings deposited by atmospheric plasma spraying," J. Mater. Process. Technol., 2002.

[9] Various, "Fast-regime fluidized bed machining of thermally sprayed TiO_2/Cr_2O_3/WC-Co coatings," 2008.

[10] Various, "Material removal mechanisms in alumina coatings via superabrasive grinding," 2016.

[11] S. Kar et al., "High-speed grinding of plasma-sprayed ceramic coatings," 2017.

[12] M. Bhattacharya et al., "Machinability of sintered hydroxyapatite ceramics by conventional drilling," 2003.

[13] J.D. Majumdar et al., "Drilling of HAp–Yttrium Phosphate composite using HSS and carbide drills," 2016.

[14] M. Bhattacharya et al., "Drilling of β-TCP/YP composite using HSS and solid carbide drills," 2016.

[15] S. Das et al., "Ultrasonic machining of hydroxyapatite bio-ceramics for surface quality optimization," 2016.

[16] A.K. Mehar et al., "Taguchi mixed-level design on HA–polypropylene composite plates drilling," Mater. Today: Proc., 2018.

[17] A.K. Mehar et al., "Taguchi L27 OA on CNC drilling of HA-PC/HA-PS composites for thrust force and surface roughness optimization," 2020.

[18] Various, "HA-mixed EDM for simultaneous machining and coating of metallic biomaterials," 2021.

[19] Various, "HA-mixed EDM on SS 316L substrate: recast layer and surface modification," 2024.

[20] G.C.S. Meireles et al., "Water-jet laser drilling of biomorphic HA scaffolds for enhanced porosity," 2024.

[21] M. Katto et al., "Excimer laser ablation of sintered hydroxyapatite," 2006.

[22] S.R. Paital et al., "Excimer laser (KrF) treatment of dense HA ceramics for surface texturing," 2003.

[23] S.H. Um et al., "Simultaneous synthesis and coating of HAp via nanosecond laser surface treatment," 2020.

[24] D. Ke et al., "Gradient HA on Ti6Al4V by LENS and plasma spray for enhanced coating adhesion," 2019.

[25] D. Buser, R. Benetti et al., "Laser-ablated Ti implants with thin HA coating for enhanced osseointegration," 2012.

[26] G.E. Pecora et al., "Removal torque evaluation of laser-modified and HA-coated Ti implants in rabbit model," 2009.

[27] R.B. Heimann, "Plasma-Sprayed Hydroxylapatite-Based Coatings: Chemical, Mechanical, Microstructural, and Biomedical Properties," J. Thermal Spray Technology, vol. 25, pp. 827–850, 2016.

[28] S. Hussain et al., "Characterization and tribological behaviour of Indian clam seashell-derived hydroxyapatite coating applied on titanium alloy by plasma spray technique," J. Mech. Behav. Biomed. Mater., 2023.

[29] K. de Groot et al., "Plasma sprayed coatings of hydroxylapatite," J. Biomed. Mater. Res., vol. 21, pp. 1375–1381, 1987.

[30] L.L. Hench, "Bioceramics: From Concept to Clinic," J. Am. Ceram. Soc., vol. 74, pp. 1487–1510, 1991.

[31] Y. Nattawit et al., "Highly bioactive hydroxyapatite coating made by flame spray technique," Surf. Coat. Technol., 2023.

[32] M. Akram et al., "Extracting hydroxyapatite and its precursors from natural resources," J. Mater. Sci., vol. 49, pp. 1461–1475, 2014.

[33] P.J. Ross, "Taguchi Techniques for Quality Engineering," McGraw-Hill, 1996.

[34] J.L. Deng, "Introduction to Grey System Theory," J. Grey System, vol. 1, pp. 1–24, 1989.

[35] C.L. Lin, "Use of the Taguchi method and grey relational analysis to optimize turning operations," J. Mater. Process. Technol., vol. 154, pp. 237–244, 2004.

[36] Minitab Support, "Taguchi Design: Methods and Formulas," https://support.minitab.com.

[37] ASTM C633-13, "Standard test method for adhesion or cohesion strength of thermal spray coatings," ASTM International.

[38] ASTM E1920-03, "Standard guide for metallographic preparation of thermal sprayed coatings," ASTM International.

[39] Taylor Hobson Ltd., "Surtronic 25 Operating Manual," Technical Documentation.

[40] S. Hussain et al., "Synthesis of hydroxyapatite from Indian clam seashells by hydrothermal method," Mater. Today: Proc., 2022.

[41] S. Hussain, Z.A. Shah, K. Sabiruddin, and A.K. Keshri, "Characterization and tribological behaviour of Indian clam seashell-derived hydroxyapatite coating applied on titanium alloy by plasma spray technique," J. Mech. Behav. Biomed. Mater., vol. 137, p. 105550, 2023.

[42] https://www.orchid-ortho.com/Services/Manufacturing/Bone-In-Growth-Coating